Interference Measurements of Non-Abelian $e/4$ & Abelian $e/2$ Quasiparticle Braiding

R. L. Willett,[1,*,†] K. Shtengel,[2] C. Nayak,[3,4] L. N. Pfeiffer,[5] Y. J. Chung,[5] M. L. Peabody,[1] K. W. Baldwin,[5] and K. W. West[5]

[1]*Nokia Bell Labs, Murray Hill, New Jersey 07974, USA*
[2]*Department of Physics and Astronomy, University of California, Riverside, California 92521, USA*
[3]*Microsoft Quantum, Elings Hall, University of California, Santa Barbara, California 93106, USA*
[4]*Department of Physics, University of California, Santa Barbara, California 93106, USA*
[5]*Department of Electrical Engineering, Princeton University, Princeton, New Jersey 08544, USA*

(Received 10 September 2021; revised 21 October 2022; accepted 3 January 2023; published 1 March 2023)

The quantum Hall states at filling factors $\nu = 5/2$ and $7/2$ are expected to have Abelian charge-$e/2$ quasiparticles and non-Abelian charge-$e/4$ quasiparticles. The non-Abelian statistics of the latter is predicted to display a striking interferometric signature, the even-odd effect. By measuring resistance oscillations as a function of the magnetic field in Fabry-Pérot interferometers using new high-purity heterostructures, we for the first time report experimental evidence for the non-Abelian nature of excitations at $\nu = 7/2$. At both $\nu = 5/2$ and $7/2$, we also examine, for the first time, the fermion parity, a topological quantum number of an even number of non-Abelian quasiparticles. The phase of observed $e/4$ oscillations is reproducible and stable over long times (hours) near both filling factors, indicating stability of the fermion parity. At both fractions, when phase fluctuations are observed, they are predominantly π phase flips, consistent with either fermion parity change or change in the number of the enclosed $e/4$ quasiparticles. We also examine lower-frequency oscillations attributable to Abelian interference processes in both states. Taken together, these results constitute new evidence for the non-Abelian nature of $e/4$ quasiparticles; the observed lifetime of their combined fermion parity further strengthens the case for their utility for topological quantum computation.

DOI: 10.1103/PhysRevX.13.011028

Subject Areas: Condensed Matter Physics, Quantum Information, Strongly Correlated Materials

I. INTRODUCTION

The idea of fault-tolerant topological quantum computation is premised on both the existence of non-Abelian anyons and our ability to manipulate them [1]. Fractional quantum Hall (FQH) states are the best established examples of topological phases with FQH states at filling fractions $\nu = 5/2$ and $7/2$ being arguably the strongest candidates for non-Abelian phases. They are predicted to have non-Abelian charge-$e/4$ excitations if their ground states are in either the Moore-Read Pfaffian [2], anti-Pfaffian [3,4], or particle-hole-symmetric Pfaffian (PH Pfaffian) [5–8] universality class. In addition to their electrical charge, these excitations also carry the non-Abelian topological charge of Ising anyons [1,9], which can be understood as the presence of a Majorana zero mode [10]. A combined quantum state of a pair of such anyons (known as a fusion channel) can be viewed as an Abelian charge-$e/2$ excitation (which is a "conventional" Laughlin quasiparticle, i.e., a fractionally charged quasiparticle corresponding to an insertion of one additional flux quantum), either with or without a neutral fermion [11]; see Fig. 1. The presence or absence of the neutral mode determines the fermion parity of the state. The nature of these excitations—both their charge and statistics—can be probed by interferometry experiments [12–17]. The non-Abelian properties of the $e/4$ quasiparticles should manifest themselves in the even-odd effect, whereby the interference between two different paths for an $e/4$ quasiparticle is switched on or off whenever the difference between the paths encircles, respectively, an even or odd number of $e/4$ quasiparticles; see Fig. 1. In the meantime, the Abelian $e/2$ quasiparticle should show interference regardless of the number of encircled quasiparticles, with a pattern similar to other Laughlin quasiparticles. In a realistic Fabry-Pérot interferometer, the interference pattern

*Present address: R. L. Willett, Nokia Bell Labs, Room 1d-217, Murray Hill, New Jersey 07974, USA.
†Corresponding author.
robert.willett@nokia.com

Published by the American Physical Society under the terms of the Creative Commons Attribution 4.0 International license. Further distribution of this work must maintain attribution to the author(s) and the published article's title, journal citation, and DOI.

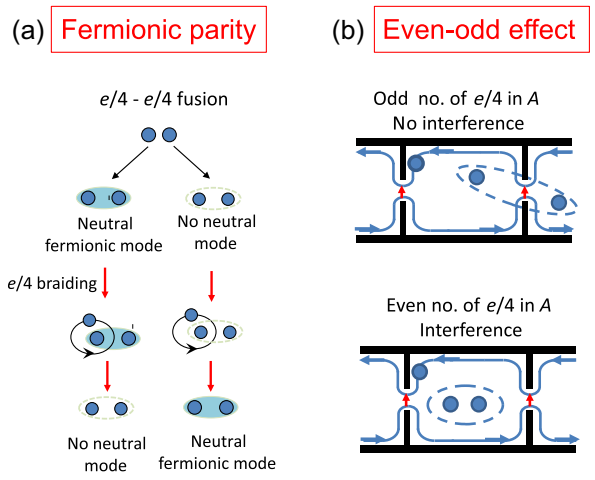

FIG. 1. Fermion parity and the non-Abelian even-odd effect. (a) The fusion of two non-Abelian $e/4$ quasiparticles has two possible outcomes, one with and one without a neutral fermionic mode. The fermion parity is a quantum number associated with an even number of such quasiparticles. It is changed when one constituent $e/4$ quasiparticle is braided by an external $e/4$ quasiparticle. (b) When $e/4$ quasiparticles backscatter from the lower to the upper edge of the Hall bar at the two constrictions, the outcome depends dramatically on the parity of $e/4$ quasiparticles inside the interferometer. If their number is even, quasiparticles propagating along two possible paths interfere akin to the familiar double slit interference. If this number is odd, the interference disappears since with each tunneling quasiparticle the fermion parity is either switched or not, depending on which path is taken. The final quantum states are therefore orthogonal to one another, which precludes interference.

should consist of oscillations due to all types of charged quasiparticles present in the system. It is the goal of this study to experimentally determine the full set of observed oscillation frequencies at $\nu = 5/2$ and $7/2$ and to compare the observed frequencies with theoretical predictions based on the braiding properties of the $e/2$ and $e/4$ quasiparticles.

Previous interferometry experiments at $\nu = 5/2$ [18–22] have observed resistance oscillations consistent with charge-$e/4$ and charge-$e/2$ excitations displaying, respectively, non-Abelian braiding and Abelian braiding statistics. Meanwhile, tunneling [23] and charge-sensing measurements [24] at $\nu = 5/2$ have found signatures of $e/4$ quasiparticles but no indication of $e/2$ quasiparticles. At the same time, shot-noise measurements [25] found evidence for $e/4$ quasiparticles and indicated a crossover from $e/4$- to $e/2$-dominated behavior in different temperature and voltage ranges [26–28]. These measurements did not probe the braiding statistics of the excitations, only their electrical charge. By contrast, interferometry measurements can provide information about both the charge and the braiding statistics of the quasiparticles. A recent measurement of the thermal Hall conductivity [29] is an indirect probe of the topological order of the bulk and, therefore, an indirect measure, at best, of the presence of quasiparticles with non-Abelian braiding statistics in the bulk.

This study presents two important new findings: (i) interferometric signatures consistent with the non-Abelian even-odd effect at filling factor $\nu = 7/2$, and (ii) stable (over hours or even days) interference oscillations consistent with the even-odd effect at both $\nu = 5/2$ and $7/2$, where at both filling factors sporadic interruptions of this stability take the form of phase jumps by π indicative of either the fermion parity change or change in the number of the enclosed $e/4$ quasiparticles.

The key experimental advance underpinning the study presented here is the development of a new class of ultra-high-mobility AlGaAs heterostructures in which the Al alloy layers are purified to the extreme, promoting stronger electron-electron correlations, and thus more robust quantum Hall states than previously attained. This improvement in the material purification also results in a substantially larger amplitude of resistance oscillations observed in new interferometer devices. Specifically, in addition to providing more solid evidence for the non-Abelian nature of the $\nu = 5/2$ state, we report the first experimental evidence in support of the similar nature of the $\nu = 7/2$ state. Furthermore, oscillations consistent with the even-odd effect associated with transport by non-Abelian charge-$e/4$ quasiparticles are stable in the timescales of hours or even days. When an instability occurs, it takes the form of a π phase shift consistent with the change of either the fusion channel of the enclosed non-Abelian anyons or their number, thus providing further evidence for the non-Abelian nature of the states. Irrespective of the mechanism for these phase shifts, they are observed to occur infrequently. This strengthens the case for using such FQH systems as a platform for topological quantum computation.

Both heterostructure and interferometer designs used in this study allow us to address another potential issue that has been plaguing earlier interference studies. Specifically, resistance oscillations of a mesoscopic quantum Hall island can be due to some combination of the Aharonov-Bohm (AB) and Coulomb blockade effects. The latter effects are expected to dominate in smaller devices [30], and some early results [31–33] are consistent with this. However, several aspects of our heterostructure design work to suppress Coulomb effects. Most importantly, we use special heterostructures that contain additional conducting layers able to screen the long-range Coulomb interactions (see Sec. S2 of the Supplemental Material [34]). This layering promotes AB oscillations even in relatively small quantum Hall interferometers at $\nu = 5/2$ and $7/3$ [18–22]; it is akin to employing surface top gates used for the same purpose in previous Fabry-Pérot interferometry studies [35,36]. Despite these additional conducting layers, our devices allow illumination of the samples to achieve the necessary high quality needed to observe $\nu = 5/2$ and $\nu = 7/2$ states. The case for AB oscillations aided by

parallel conductors is supported by recent measurements [37] at $\nu = 1/3$. A second important design feature of our devices is their high electron densities 4×10^{11} cm^{-2}, which also suppress Coulomb effects. In addition, our measurements employ large-aperture interferometers that contribute to further suppression of Coulomb blockade effects.

The manuscript is organized as follows. In Sec. II, we present an extensive review of quantum Hall interferometry, emphasizing the expected periodicities of the AB oscillations for both Abelian and non-Abelian quasiparticles expected at $\nu = 5/2$ and $7/2$. For non-Abelian quasiparticles, we focus on the consequences of the existence of two fusion channels corresponding to the two possible fermion parities that may be contained within the loop (displayed schematically in Fig. 1). In Sec. III, we turn to the description of the devices and experimental methods used to probe these predictions. We present evidence in support of the Aharonov-Bohm mechanism as the dominant mechanism behind the interference oscillations. Section IV, is dedicated to our principal experimental results—stable oscillations observed at $\nu = 5/2$ and $7/2$, which demonstrate occasional π phase shifts. In Sec. IV A we present full power spectra of these oscillations at $\nu = 7/2$ and identify spectral peak positions observed at these filling fractions. In Sec. IV B, we present evidence of the temporal stability of non-Abelian quasiparticle fusion. We observe occasional π phase shifts that we attribute to changes in the fusion channel (fermionic parity) or the parity of the enclosed non-Abelian quasiparticles. In Sec. IV C, we present similar findings for $\nu = 5/2$. In addition, in Sec. IV D we focus on the signatures of Abelian braiding processes and demonstrate the ability to control a specific component of the interference spectrum attributable to different braiding processes. We conclude that, taken together, these data significantly strengthen the case for both the non-Abelian nature of the FQH states at $\nu = 5/2$ and $7/2$ (while providing the first such experimental evidence for the latter state) and for their potential applications for quantum-information processing.

II. INTRODUCTION TO FRACTIONAL QUANTUM HALL INTERFEROMETRY

In this section, we describe various types of resistance oscillations that can be observed in quantum Hall interferometers. We review the oscillations expected to be observed in magnetic field sweeps in Abelian quantum Hall states with contributions from both the Aharonov-Bohm and statistical phases. We explain how this picture is altered if the state in question is non-Abelian and focus on the role the fermionic parity plays in this case. We also mention an alternative mechanism for resistance oscillations originating from breathing of Coulomb-dominated electron droplets. As we discuss, these different phenomena can be distinguished by their resistance oscillation spectra.

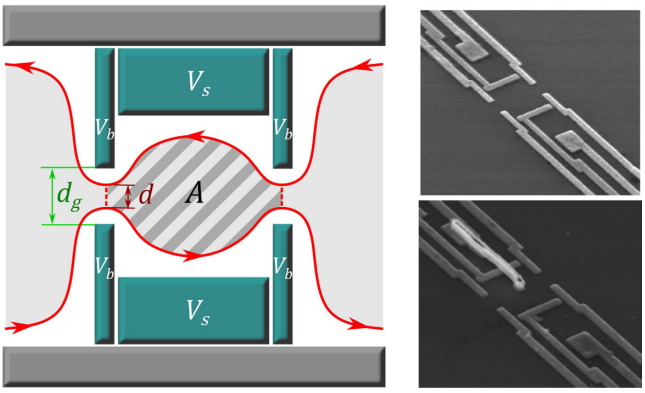

FIG. 2. Schematic and electron-micrograph images of interference devices. The interferometer is defined by surface gates operated at voltages V_b and V_s that deplete the electron population below them. Currents propagate along the edges separating the incompressible QH liquid (shaded) and the depleted regions; contacts diffused into the heterostructure away from the device are used to measure resistance across the device longitudinally R_L and in Hall configuration across the device R_D. Edge current can backscatter at one of the two constrictions resulting in interference of the two paths. The area between the two paths—the active area A of the interferometer—is indicated by stripes; the filling factor within the active area is the same as in the shaded bulk regions on either side. Device images show one device with no structure inside area A (top, device type (a) and another one with a top gate central dot (device type b). In each device, the lithographic separation d_g of gates defining the constrictions is approximately 1 μm. The actual tunneling distance between the edge currents d is controlled by the gate voltage V_b.

Fabry-Pérot interferometry in the two-dimensional electron gas in the quantum Hall regime is due to interference between two different paths by which electrical current can flow from source to drain along edge states and across constrictions (see Fig. 2). The interference pattern is thus determined by the total phase difference accumulated along the two paths, which in turn consists of both the Aharonov-Bohm phase determined by the charge of the propagating quasiparticles and the enclosed flux, and the statistical contribution determined by the statistics of the quasiparticles and the number and type of the quasiparticles enclosed between the two paths. This overall phase difference can be changed experimentally by changing either the enclosed flux or the number of quasiparticles within the interferometer loop. As we discuss in more detail in Sec. S1 of the Supplemental Material [34], for Abelian quasiparticles, this change is given by

$$\Delta\gamma_{e^*} = 2\pi\left(\frac{\Delta\Phi}{\Phi_0}\right)\left(\frac{e^*}{e}\right) + 2\theta_{e^*}\Delta N_{e^*}. \tag{1}$$

In this expression, $\Delta\Phi$ is the change in the encircled flux, $\Phi_0 = hc/e \approx 41$ G μm^2 is the flux quantum, and ΔN_{e^*} is

the change in number of the enclosed quasiparticles of charge e^*. Their braiding statistics is described by statistical angle θ_{e^*}—a phase acquired by the wave function upon counterclockwise exchange of two identical quasiparticles.

A key difference between the Abelian interference described by Eq. (1) and non-Abelian interference is that in the former case both the encircled flux and the number of enclosed quasiparticles play a similar role: They simply contribute to the phase difference between the two interfering paths. However, if the interfering quasiparticles are non-Abelian, the number of enclosed quasiparticles does not just contribute to the phase difference, it can change the amplitude of the interference term [38]. The most dramatic manifestation of this property is the even-odd effect predicted for the interference of $e/4$ quasiparticles in non-Abelian $\nu = 5/2$ or $7/2$ QH states. Specifically, the interference is only possible when the number of encircled $e/4$ quasiparticles is even, whereas no Aharonov-Bohm oscillations should be observed if the number is odd; see Fig. 1.

According to Eq. (1), two parameters can potentially be varied in interferometric studies: the encircled flux and the number of enclosed quasiparticles. While varying them independently may seem experimentally hard, the variation of different combinations of them is achieved by (i) varying the side gate (V_s) at fixed magnetic field [19–21], and (ii) varying the magnetic field at fixed gate voltage [22]. The active area A in an interferometer—the area encircled by the current paths—is defined by surface gates. Varying the applied voltages on these gates changes this area; consequently, it changes both the enclosed flux and the number of $e/4$ quasiparticles randomly localized within the area. This method has shown signatures of both $e/2$ and $e/4$ quasiparticles and also demonstrated a pattern of oscillations consistent with the non-Abelian nature of the latter, specifically the aforementioned even-odd effect [13,14] whereby the Aharonov-Bohm oscillations associated with electrical transport by $e/4$ quasiparticles are observed only when an even number of $e/4$ quasiparticles is localized within the interferometer loop. In the meantime, Aharonov-Bohm oscillations associated with electrical transport by $e/2$ quasiparticles are always present.

When the magnetic field is varied with fixed gate voltage, the enclosed magnetic flux number and the enclosed quasiparticle number change in tandem (see Sec. S1 of the Supplemental Material [34]). Specifically, in the simplest model we assume that the active area of the interferometer is independent of the magnetic field (thus, discounting the possibility of so-called Coulomb domination [17,39]; see Sec. S1 of the Supplemental Material [34] for more details). In this case, the change in the number of bulk quasiparticles in response to the change in flux $\Delta\Phi$ is given by $\Delta N_{e^*} = -(\Delta\Phi/\Phi_0)(\nu e/e^*)$, resulting in

$$\Delta\gamma_{e^*} = \left(\frac{\Delta\Phi}{\Phi_0}\right)\left[2\pi\left(\frac{e^*}{e}\right) - 2\theta_{e^*}\left(\frac{\nu e}{e^*}\right)\right]. \tag{2}$$

The putative non-Abelian nature of $e/4$ quasiparticles should result in specific small-period oscillations centered near $5f_0$ for the $\nu = 5/2$ state (and $7f_0$ for the $\nu = 7/2$ state), with $f_0 = 1/\Phi_0$ being the oscillation frequency corresponding to the period of one flux quantum. These small period oscillations are a manifestation of the even-odd effect (illustrated schematically in Fig. 1; see also schematic for fermion parity) driven by the systematic variation of the $e/4$ quasiparticle number as the magnetic field is changed (B-field sweep): The interference of $e/4$ quasiparticles traversing the interferometer should be on or off if there is an even or odd number of $e/4$ quasiparticles within the loop. Repeated switching between these regimes results in additional resistance oscillations. The corresponding period is determined by the flux needed to increase the number of $e/4$ quasiparticles within the active area of the interferometer by two, namely, a period of $2\Phi_0 e^*/\nu e = \Phi_0/5$ at $\nu = 5/2$ and $\Phi_0/7$ at $\nu = 7/2$. Such high-frequency peaks should be an unmistakable signature of non-Abelian statistics, and they were first reported in the earlier study [22] at $5/2$ filling.

However, a more complicated picture emerges when all quasiparticle types are considered. Specifically, if both $e/4$ and $e/2$ excitations are present, one should observe oscillations due to all permutations of interfering and enclosed quasiparticles. A straightforward generalization of Eqs. (1) and (2) for the Abelian phase acquired by interfering quasiparticles of type a encircling bulk quasiparticles of type b is given by

$$\begin{aligned}\Delta\gamma_{ab} &= 2\pi\left(\frac{\Delta\Phi}{\Phi_0}\right)\left(\frac{e_a}{e}\right) + 2\theta_{ab}\Delta N_b \\ &= \left(\frac{\Delta\Phi}{\Phi_0}\right)\left[2\pi\left(\frac{e_a}{e}\right) - 2\theta_{ab}\left(\frac{\nu e}{e_b}\right)\right].\end{aligned} \tag{3}$$

Direct application of this expression results in oscillation periods of Φ_0 for $e/4$ quasiparticles interfering around $e/2$ quasiparticles and $\Phi_0/2$ for the $e/2$ quasiparticles interfering around either $e/4$ or $e/2$ quasiparticles. Finally, the interference of $e/4$ around $e/4$ quasiparticles would naively result in the period of $4/9\Phi_0$ for the Moore-Read Pfaffian state and $4/11\Phi_0$ for the anti-Pfaffian state (see Sec. S1 of the Supplemental Material [34] for more details). However, this is not the case since in both states the $e/4$ excitations are actually non-Abelian. Therefore, the interference turns on and off with each shift $\Delta N_{e/4} = \pm 1$, resulting in the aforementioned small period of $\Delta\Phi = \Phi_0/5$.

When the number of bulk $e/4$ excitations is even, the interference is not simply governed by $\theta_{e/4}$; it also depends on the fusion channel of the enclosed quasiparticles. There are three basic possibilities: (i) The fusion channel, which determines the fermion parity, is fixed by the energetics and remains largely stable during the magnetic field sweep across the $\nu = 5/2$ plateau, (ii) the fusion channel is

random but its autocorrelation time is longer or comparable to the time it takes to change the flux by one flux quantum, and (iii) the fusion channel fluctuates rapidly on the timescale of changing the flux by $\Delta\Phi = \Phi_0$. Focusing on the first scenario, let us assume that the net fusion channel of the bulk quasiparticles is always trivial. Physically, this means that from the point of view of interference, the bulk is equivalent to a collection of $e/2$ Laughlin quasiparticles, which would result in the aforementioned Abelian factor in the interference pattern, with period of Φ_0 irrespective of the exact nature of the $\nu = 5/2$ state. The net result would be a convolution of non-Abelian $5f_0$ and Abelian f_0 oscillations, resulting in spectral peaks at $4f_0$ and $6f_0$. Were the fusion channel to contain a fermion instead, the bulk quasiparticles would be in a different fermion parity state, and the overall phase of Abelian oscillations would shift by π with no change in the oscillation period. In the second scenario, the fluctuations in the fusion channel—fluctuations in the fermion parity—would scramble the f_0 component (due to random π phase shifts throughout the magnetic field sweep), thus eliminating the beats, resulting in a single spectral peak at $5f_0$. Finally, in the third scenario, the interference of charge-$e/4$ excitations around other $e/4$ excitations would be eliminated entirely: Their interference is suppressed for odd numbers of enclosed $e/4$ quasiparticles by their non-Abelian nature and for even numbers by rapid phase fluctuations.

Note that the first and second scenarios may actually coexist within a sweep across the entire $\nu = 5/2$ plateau: One could envision, e.g., a situation whereby the fermion parity is stable near the middle of the plateau while becoming progressively less stable closer to its margins, where the concentration of the bulk quasiparticles becomes larger and hence their typical distance to the edge smaller. The latter scenario would in turn enhance tunneling of neutral fermions between the edge and the localized quasiparticles, scrambling the well-defined fermion parity in the bulk [40]. In such a case, one would find oscillation peaks at $4f_0$ and $6f_0$ near the middle of the plateau and $5f_0$ closer to its flanks.

We should note, however, that in the Coulomb-dominated regime another mechanism for generating these high-frequency spectral features may arise: Specifically, one could imagine a scenario whereby the active area of an interferometer "breathes" with the period corresponding to the introduction of additional Abelian $e/2$ quasiparticles in order to minimize the energy of the QH droplet that defines the active area—the period exactly matching that of the non-Abelian even-odd effect. Such a mechanism, which is described in more detail in Sec. S1 of the Supplemental Material [34], would rely solely on the energetics of the $e/2$ quasiparticles inside the interferometer and thus be oblivious to the nature of charge-$e/4$ quasiparticles. Therefore, a convincing proof of the non-Abelian statistics of the charge-e/4 quasiparticles must rule out this scenario; we address this important issue in the following section as well as in Sec. S4b of the Supplemental Material [34].

TABLE I. Possible mechanisms and spectral features of resistance oscillations at $\nu = 5/2$ and $7/2$.

Mechanism		$\nu = 5/2$	$\nu = 7/2$
Non-Abelian even-odd effect	Stable fermionic parity	$(5 \pm 1)f_0$	$(7 \pm 1.5)f_0$
	Slow parity fluctuations	$5f_0$	$7f_0$
	Fast parity fluctuations	…	…
$e/4 \odot e/2$		f_0	$1.5f_0$
$e/2 \odot e/4, e/2$		$2f_0$	$3f_0$
Coulomb-dominated breathing		$5f_0$	$7f_0$

These considerations can also be applied to $\nu = 7/2$, where the charge-$e/4$ quasiparticle is similarly expected to obey non-Abelian statistics. Upon magnetic field sweep, the non-Abelian even-odd effect will manifest itself through the resistance oscillations with period corresponding to the magnetic field increment needed to change the number of $e/4$ quasiparticles by two, which in terms of flux corresponds to the period of $2\Phi_0 e^*/(\nu e) = \Phi_0/7$ or frequency $7f_0$ in the Fourier spectrum of the resistance oscillations. These oscillations may be then modulated by the frequency of $1.5f_0$ corresponding to $e/4$ quasiparticles interfering around $e/2$ quasiparticles, according to Eq. (3). Thus, spectral peaks are expected at either $7f_0$ or $7f_0 \pm 1.5f_0$, depending upon the fermion parity stability and the Fourier transform window; see Table I for the summary. Finally, the spectrum could also display a peak corresponding to $e/2$ interfering around $e/2$, and from Eq. (2) this frequency would be $3f_0$. The $7/2$ spectrum could then be comprised of peaks at either $1.5f_0$, $5.5f_0$, and $8.5f_0$ or at $1.5f_0$ and $7f_0$ (or, perhaps, at all of those), and in addition, there might be a spectral peak at $3f_0$ as well.

Yet, just like in the case of $\nu = 5/2$, in order to ascertain the non-Abelian nature of high-frequency oscillations at $\nu = 7/2$, one must rule out the possibility of the aforementioned "breathing" of the active area of the interferometer, which in the Coulomb-dominated regime could also produce resistance oscillations with frequency $7f_0$. Fortunately, this scenario would not be specific to $\nu = 5/2$ and $7/5$; it would result in similar high-frequency oscillations in nearby Abelian fractional quantum Hall states and thus can be eliminated from consideration absent such oscillations. In the next section, we provide experimental details that support eliminating this mechanism.

In summary, in the Aharonov-Bohm regime the observed resistance oscillations should be a combination of interference patterns resulting from charge-$e/4$ Ising anyon encircling another $e/4$ Ising anyon; a charge-$e/2$ Abelian anyon encircling another charge-$e/2$ Abelian anyon as well

as both types of anyons encircling the other kind. In addition, the phase of the charge-$e/4$ quasiparticle interference should depend on the parity of neutral fermions inside the loop. At $5/2$ filling, the first type of process leads to a resistance that oscillates with magnetic flux with frequency $5f_0$, whereas at $7/2$ the corresponding frequency is $7f_0$. The $e/2$-$e/2$ interference in these states should result in oscillations with frequency $2f_0$ and $3f_0$, respectively. We show later that the amplitude of these oscillations can be tuned independently of $e/4$ interference oscillations, effectively allowing for them to be turned on or off. Finally, the interference of $e/4$ quasiparticles around Laughlin $e/2$ quasiparticles produces oscillations with frequency f_0 at $\nu = 5/2$ and $1.5f_0$ at $\nu = 7/2$; its convolution with the first type of process results in oscillation frequencies $5f_0 \pm f_0$ and $7f_0 \pm 1.5f_0$, respectively. The stability of the fermion parity should determine whether a measured high-frequency spectral peak is split in this manner or remains centered at $5f_0$ or $7f_0$ (with an additional possibility of both scenarios occurring within the same plateau). Table I presents an abbreviated summary of these predictions.

Irrespective of those details, once the Coulomb-dominated regime is eliminated in favor of the Aharonov-Bohm regime, an appearance of such high-frequency spectral features in the magnetic-field-driven AB oscillations in the vicinity of $5f_0$ at $\nu = 5/2$ and $7f_0$ at $\nu = 7/2$ should be an unmistakable signature of the non-Abelian nature of those states. Observations of high-frequency spectral peak(s) both in the previous [22] and present studies can then be interpreted not only as a confirmation of the non-Abelian nature of the $\nu = 5/2$ state but also as a validation of the results of the earlier side-gate studies as the main conceptual criticism of those was rooted in doubts about the fusion channel stability [40].

III. METHODS

Two wafer types are employed in our study: shielded-well and doping-well wafers; see Sec. S2 of the Supplemental Material [34]. The shielded-well densities are all near 4×10^{11} cm^{-2}; the single-doping-well wafer density is 2.7×10^{11} cm^{-2}. Note that the electron densities of these wafers, and in particular, of the shielded-well wafers, are substantially larger, by factors of 1.5 to 7, than those used in other edge interferometry measurements [31,35–37,41,42]. Wafer mobilities all exceed 25×10^6 cm$^2/Vs$. Table S2-T1 of the Supplemental Material [34] contains details of the density and respective wafer mobilities. All measurements are performed in dilution refrigerators with base temperatures 20 to 25 mK. Unless otherwise stated, the measurement temperature is at or near these base temperatures.

Several essential unique experimental methods contribute to the results in this study and are outlined here, followed by a description of the interference device operation needed to understand the results. Specific heterostructure designs and growth features are crucially important: breakthrough improvement in the purity of Al in the GaAs/AlGaAs heterostructure quantum wells, consequently increasing the electron correlation effects, and placement and electron population of conducting layers parallel to the principal quantum well to suppress Coulomb blockade. Aluminum purity in our heterostructures is improved by first assessing the oxygen impurity levels in the heterostructure AlGaAs layers [43], then developing methods of off-line Al-effusion furnace bakes to reduce these charged impurities. These bakes ultimately result in AlGaAs barrier material used in the heterostructures of this study with about 8 times fewer impurities than previous material [44]. In these extreme high-purity materials, and in previously grown heterostructures [18–22], a unique multiple conduction layering structure is employed for materials used in our interference measurements. Parallel to the principal quantum well both above and below, poorly conducting layers are grown, which suppresses Coulomb blockade or domination of the interferometer's laterally confined electron layer in the principal well. (A similar charge-shielding approach was employed in recent studies [41] to suppress Coulomb domination in the low-density samples.) These parallel layers are populated differentially by the doping layers, and illumination of the samples at low temperatures contributes further to that population: Such illumination of the samples is distinctly unique to our method, as is the aluminum purification, versus all others [23–25,29–33,37,41]. Different illumination, cooldown, and gating histories for a given sample can produce different electron populations in the layers. Each such history is numbered and in the results sections is referred to as the preparation number for each sample. See Sec. S2 of the Supplemental Material [34] for details on heterostructure construction and illumination and on the Al purification method for this study. Also see Sec. S2 of the Supplemental Material [34] for details of the preparation histories applied to the samples used in our measurements.

An interference device is shown schematically in Fig. 2. The top gates are charged to a negative voltage sufficient to deplete the underlying electron layer. At high magnetic fields, as prescribed for filling factor $\nu = 5/2$ or $7/2$ (filling factor ν being the ratio of the electron areal density to the magnetic flux density), the currents carrying the excitations of the fractional quantum Hall state will travel along the edge of these depleted areas, surrounding an area of the bulk filling factor ν. The important principal physical property of the interferometer device is two separated locations where these edge currents are brought in proximity of one another. At these points, backscattering from one edge to the other can occur, and with this backscattering, two different current paths are established that can interfere, as shown by the dashed lines in the schematic. The one path encircles the area marked A in the schematic, and changes in the magnetic flux number within area A or changes in the particle number within area A will cause phase accumulation

for that path (the Aharonov-Bohm and statistical phase contributions). Interference of that path and the one not entering the area A produce oscillations in the resistance measured across the interference device. The voltages on the top gates can be adjusted to promote backscattering (gates marked V_b) and to change the enclosed area A (gates marked V_s). The separation of the backscattering top gates, distance marked d_g in Fig. 2, is sufficiently large that for nominal voltages on V_b the backscattering is weak, an important feature to maintain the $5/2$ fractional Hall state contiguously from outside to inside the active area A of the interferometer. Note also that area A is ultimately the area which is enclosed by the edge states in the quantized Hall systems, and not the lithographic area. The location of the edge states is determined electrostatically and can be modified by the applied gate voltages.

Tunneling between the innermost edge currents that surround the region of bulk electron density (depicted as shaded in Fig. 2) at the two constrictions results in the interference between two possible paths for the backscattered current. Although the lithographic area is several square microns, the active area A is typically less than one square micron. The experimental evidence that the desired $\nu = 5/2$ and $7/2$ QH states persist inside the active area of the interferometer is shown in Sec. S4 of the Supplemental Material [34]. In one interferometer device type, a small dot is placed centrally in the area A and is accessed by an air bridge that extends over one of the side gates marked V_s in Fig. 2. Although such type-b devices (i.e., those with a top central gate) are present in several of the samples used in this study, the central gate is kept grounded for all the measurements and preparations for the purposes of obtaining the data presented in this paper. Also shown are electron micrographs of the interferometers.

Resistance and resistance oscillations are measured using low-noise lock-in amplifier techniques. A constant current (typically 2 nA) is driven through the 2D electron system underlying the interferometer top gate structure, and the voltage, and so resistance, is determined with a four-terminal measurement. The voltage drop along the same edge of the 2D electron system and across the device gives the longitudinal resistance R_L; across the device and across the two edges of the 2D system gives diagonal resistance R_D. Similar measurements performed away from the interferometer device yield R_{xx} and R_{xy}, respectively.

An example of longitudinal resistance R_L across an interferometer in an ultrahigh-mobility heterostructure characterized by improved Al purity is shown in Fig. 3(a). (Also see Sec. S4 of the Supplemental Material [34].) In comparison to heterostructures without improved Al purity (see Fig. 11 and Supplemental Material Fig. S5-1 [34]), this resistance trace shows sharper resistance features throughout this filling factor range. An enlargement of the R_L trace near $\nu = 7/2$ reveals a set of reproducible oscillations shown in Fig. 3(b). Their Fourier transform reveals a prominent peak at a frequency roughly 7 times that of the main spectral peak observed at an integer filling fraction, as shown in Fig. 3(c) [45]. A similar set of data for $\nu = 5/2$ is shown in Fig. 10. The analysis of these oscillations, their spectra, and their attribution to the non-Abelian even-odd effect is the main focus of this paper.

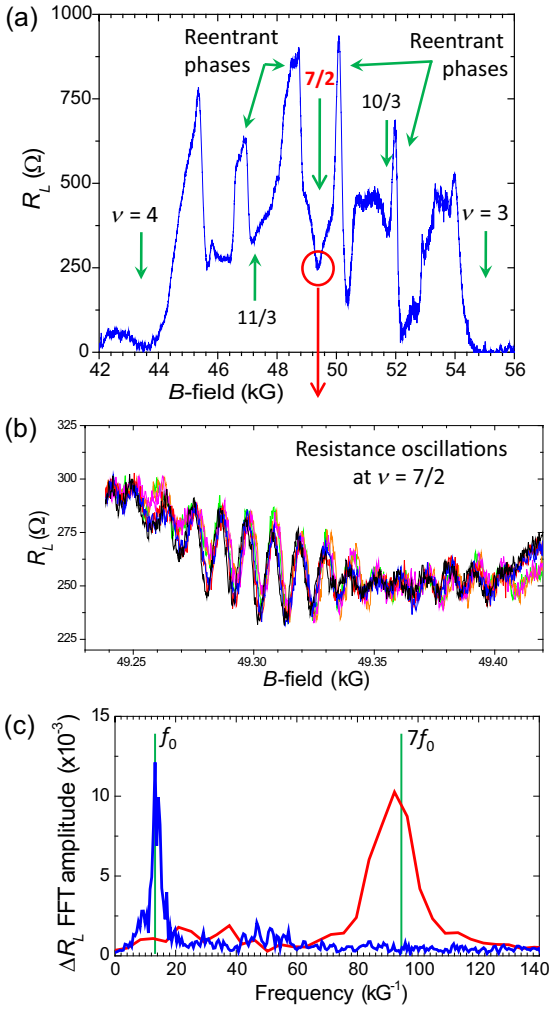

FIG. 3. (a) Longitudinal resistance R_L measured across the interferometer between filling factors $\nu = 3$ and $\nu = 4$ in an ultrahigh-mobility heterostructure. Integer and fractional quantum Hall states as well as phase-separated (nematic) states are labeled. Temperature approximately 20 mK, sample 6, preparation 16, device type b. (b) An enlargement of $R_L(B)$ near the filling factor $7/2$ demonstrating large-amplitude interference oscillations. Trace sets show oscillations near $\nu = 7/2$ for both up- and downsweeps of magnetic field B. The set of six sweeps shown here covers a time of 8.75 hours, 87.5 minutes for each directional sweep. The data demonstrate both a high level of reproducibility and stability for the time and magnetic field ranges over which the data are taken. See also Figs. S5-2–S5-4 in the Supplemental Material [34]. (c) A Fourier transform of these oscillations (red) overlayed with the Fourier transform of oscillations observed at $\nu = 3$ (blue). Vertical green lines mark the frequency f_0 of the integer spectral peak and its multiple $7f_0$, the expected frequency of the non-Abelian even-odd effect at $\nu = 7/2$.

The interference oscillations in the measured resistance are analyzed by applying fast Fourier transforms (FFT) to the data. Because the oscillations are observed near the minima of resistance of quantum Hall states, the corresponding background—the shape of the minimum—is subtracted before the FFT is applied. The subtracted background is determined equivalently by either a polynomial fit or a running large element smoothing of the minimum. By following this procedure at both integer ($\nu = 4$) and fractional ($\nu = 16/5$) filling, we can test the validity of our approach and, specifically, confirm the expectation that our interferometers operate in the Aharonov-Bohm and not Coulomb-dominated regime, thus justifying the key assumption used in deriving Eq. (2). Specifically, at the $\nu = 16/5$ FQH state, one expects a Laughlin state with $e^* = e/5$ and $2\theta_{e^*} = 2\pi/5$. Consequently, Eq. (2) predicts the phase accumulation of -6π per additional flux quantum resulting in the expected AB periodicity of $\Delta\Phi = \Phi_0/3$, which is what we observe experimentally; see Fig. 4.

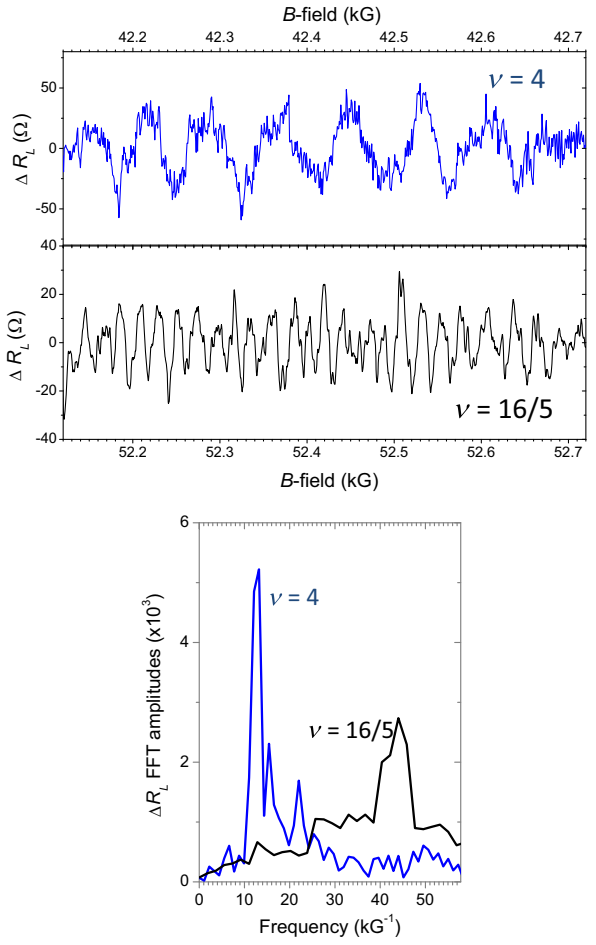

FIG. 4. A comparison of magnetic field sweeps and their Fourier transforms at $\nu = 4$ and $\nu = 16/5$ in the same sample (sample 6, preparation 25, device type b, $T \sim 20$ mK). A dominant spectral feature observed at $\nu = 16/5$ is located at approximately 3 times the frequency of the integer peak, as expected from Eq. (2).

Further evidence of the Aharonov-Bohm nature of the observed interference is provided by the "pajama plots" allowing one to trace the lines of constant phase in the B-V_s plane. For the Aharonov-Bohm oscillations, one expects these lines to have a negative slope, whereas Coulomb domination should result in a positive slope [17]; the data shown in Fig. 5 for both $\nu = 3$ and $\nu = 16/5$ clearly indicate the negative slope. (Figure 5 shows data for the same sample but different preparations; different preparations can have different active areas A which can be determined from the periodicity of interference oscillations in any of their integer QH states.) Note that while it is not entirely unreasonable to expect different energetics in integer and fractional QH states due to, e.g., different width of their edge states, it is much harder to fathom a scenario whereby two nearby fractional QH states would produce drastically different energetics. The $\nu = 16/5$ state is chosen as a prominent FQH state close to $\nu = 7/2$ whose expected Abelian nature makes the interpretation of the pajama plot sufficiently straightforward. More details on the Aharonov-Bohm nature of the interference observed at integer filling factors in our samples are presented in Sec. S4 of the Supplemental Material [34].

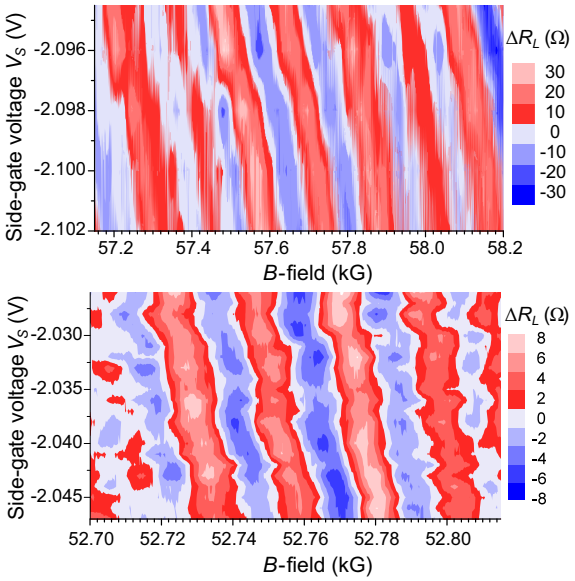

FIG. 5. Pajama plots showing the resistance oscillations at $\nu = 3$ (top) and $\nu = 16/5$ (bottom) as a function of both magnetic field B and side-gate voltage V_s consistent with the Aharonov-Bohm as opposed to Coulomb-dominated nature of observed oscillations (top panel shows sample 6, preparation 3, device b; bottom panel shows sample 6, preparation 25, device b, for which the integer oscillations are shown in Fig. 4). Note that the integer period (top panel, preparation 3) indicates an active interferometer area roughly half that of the device used in bottom panel (preparation 25), yet still demonstrating a negative phase slope indicative of the AB regime.

Finally, we also present results of a direct test that rules out a mechanism that could produce high-frequency spectral features at $\nu = 5/2$ and $7/2$ due to the oscillations of the active area of the interferometer upon changes of the magnetic field. As mentioned in the previous section and further explained in Sec. S1 of the Supplemental Material [34], such a mechanism relies on the periodic oscillations of the active area of the interferometer upon introduction therein of additional Laughlin quasiparticles. Assuming the energetics behind such a scenario do not change dramatically with the filling fraction, this mechanism would also produce high-frequency oscillations at $\nu = 7/3$—either at $f = 7f_0$ or $f = (7 \pm 2)f_0$ depending on whether the oscillations originate from merely changing the tunneling geometry or from geometric oscillations modulating quantum interference. As can be seen in Fig. 6, the FFT spectrum of the oscillations observed at $\nu = 7/3$ shows an expected peak near $2f_0$ (as determined from the integer spectrum) due to the interference of charge-$e/3$ quasiparticles but no marked features in the vicinity of $7f_0$. Crucially, the same sample shows significant features near $5f_0$ at $\nu = 5/2$ in the Fourier transform of *the same magnetic field trace* (shown in Fig. S5-6 of the Supplemental Material [34]), which rules out the Coulomb domination as the mechanism behind those oscillations.

To conclude, we like to reiterate the importance of two fundamental improvements between the new high-Al-purity shielded-wells heterostructures and the previously used shielded-well samples: The high-Al-purity samples can display a tenfold increase in the amplitude of the interference oscillations at $\nu = 7/2$ and $5/2$ compared to those previously observed in shielded-well samples, and, furthermore, the high-Al-purity materials also demonstrate sharper definition of the fractional states and the reentrant phases. This latter point is shown comparing the R_L data in Figs. 3(a) and 10 versus that of Fig. 11(a) (comparison is also made in Supplemental Material Fig. S5-1 [34]). Figure 11(a) shows only continuous evolution in R_L from the reentrant phases to, for instance, the $5/2$ minimum, in stark contrast to the abrupt changes in R_L in sweeping the magnetic field from the reentrant phases to $\nu = 5/2$ shown in Fig. 10. In Fig. 3(a) the transitions from reentrant phases to $\nu = 7/2$ are also distinct. It is posited but not proven that this relative sharpening of the reentrant features, less mixing with the target $\nu = 5/2$ and $\nu = 7/2$ states, may contribute to the larger amplitude of the oscillations at those FQH states.

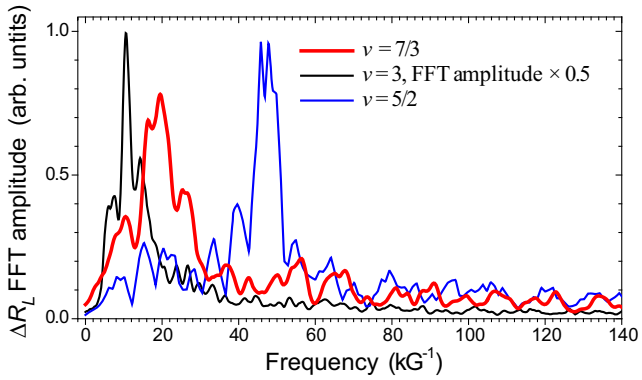

FIG. 6. Absence of significant high-frequency spectral features in the oscillations at $\nu = 7/3$ (red) in the same sample, preparation, and magnetic field trace where a marked peak in the vicinity of $5f_0$ is observed at $\nu = 5/2$ (blue). The FFT of oscillations at $\nu = 3$ in the same sample is shown in black for comparison; it establishes the fundamental frequency f_0 (sample 6, preparation 36, $T \sim 25$ mK).

IV. RESULTS

A. High-frequency spectral features of interference oscillations at $\nu = 7/2$

We now turn to our main findings, beginning with the analysis of the interference oscillations for the first time observed at $\nu = 7/2$. Figure 3(a) depicts a representative quantum Hall trace between integer fillings $\nu = 3$ and 4 observed in a higher-purity sample. It shows a well-defined feature at filling fraction = $7/2$. Focusing on the corresponding resistance minima reveals the oscillating behavior of the resistance R_L as a function of the magnetic field. As can be seen in Fig. 3(b), the observed oscillations are both prominent, with the typical amplitude of order 20 Ω, and remarkably reproducible—the figure presents the results of six different magnetic field sweeps separated from one another by hours. We should also note the generic nature of these oscillations: They are seen in different preparations and within a significant range of gate-voltage settings; see Figs. S5-3 and S5-4 of the Supplemental Material [34]. The most significant feature of these oscillations is their frequency. Indeed, as we demonstrate, it is inconsistent with any Abelian AB interference, but it is consistent with the non-Abelian even-odd effect.

In order to analyze the origin of these oscillations, we must first establish the reference frequency for our interferometer. Because we do not know the precise active area A of the interferometer, we rely on the oscillation spectra measured at integer filling factors to extract the reference frequency f_0; see, e.g., Figs. 3(c) and 4 or Fig. S5-1 of the Supplemental Material [34]. Since only electrons can interfere in the integer QH regime, the oscillation period observed as the magnetic field is swept across the integer plateau corresponds to the change of one flux quantum through the active area of the interferometer. This procedure is repeated for each sample, each cooldown, and each gate-voltage setting (see also Fig. 11, which exemplifies this procedure). Equipped with the knowledge of the electron AB oscillation frequency f_0, we proceed to examine the oscillation spectra at filling fractions $7/2$ and $5/2$.

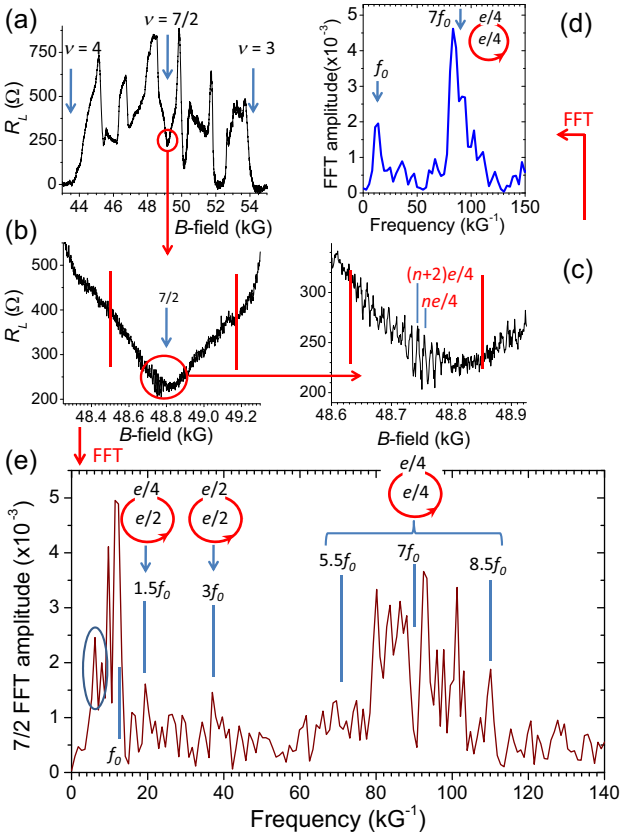

FIG. 7. Interference oscillations at $\nu = 7/2$ and their power spectra. (a) Transport between filling factors $\nu = 3$ and $\nu = 4$. (b),(c) Successive enlargements of $R_L(B)$ around the minimum at $\nu = 7/2$, demonstrating sets of interference oscillations (sample 6, preparation 8, device type b, $T \sim 20$ mK). (d) The Fourier spectrum of the sweep in panel (c) with the FFT window marked by the red vertical lines. f_0 marks the position of the FFT peak at $\nu = 3$ for this sample and preparation (see Fig. S5-1 in the Supplemental Material [34]). (e) A FFT using a larger range of B-field centered at $\nu = 7/2$ can potentially express the full complement of $e/4$ and $e/2$ braids as shown for $\nu = 5/2$ in Fig. 11. The FFT window corresponding to $\nu = 3.5 \pm 0.03$ is marked by red vertical lines in panel (b). The vertical lines marked $1.5f_0$, $3f_0$, $5.5f_0$, $7f_0$, and $8.5f_0$ are the respective multiples of f_0 identified at the integer filling, which correspond to expected features at $\nu = 7/2$ (see text for details). A broad spectral feature is centered at $7f_0$, with a sharp *minimum* developing at that frequency. Additional $\nu = 7/2$ spectra are shown in Fig. 13(b) and in Sec. S5c of the Supplemental Material [34], all demonstrating a large spectral feature centered at their respective $7f_0$ frequencies, as expected for non-Abelian $e/4$ at $\nu = 7/2$.

Having established the reference frequency f_0, we focus our attention on the interference signal at $\nu = 7/2$ shown in Fig. 3. A crucial parameter in the analysis of the resistance oscillations is the width of the Fourier-transform window. Figure 7 shows a series of successive enlargements of the resistance minimum at this filling and the corresponding Fourier transforms. The measurements presented here are done using a different preparation of the same sample that was used for the measurements in Fig. 3. Similar to what is shown in Fig. 3, using the narrower FFT window [marked in the last of these enlargements, Fig. 7(c)] results in a prominent spectral peak seen in Fig. 7(d) at approximately 84 kG^{-1} (or approximately 87 kG^{-1} if measured as a midpoint at half height), the frequency of easily identifiable reproducible oscillations shown in Fig. 7(c), as well as Fig. 3(b). The reference frequency f_0 is determined to be approximately 13.0 ± 0.5 kG^{-1} in this sample, so the observed spectral peak corresponds to $7f_0$ within reasonable precision—the very frequency expected for the even-odd effect in this quantum Hall state. A larger Fourier-transform window bounded by vertical red bars in Fig. 7(b) reveals lower-frequency features in the Fourier spectrum as can be seen in Fig. 7(e). It also points toward a more complex structure of the spectral peak centered at $7f_0$, which we discuss later.

B. Temporal stability of oscillations

One of the remarkable features of the observed oscillations attributable to the non-Abelian $e/4$ quasiparticles is their temporal stability. Generally, there are two ways of inferring the fermion parity stability: (1) direct observation of the phase stability of the $5f_0$ and $7f_0$ frequency oscillations, respectively, at $\nu = 5/2$ and $7/2$, and (2) indirect inference via the presence or absence of spectral properties, split peaks at $(5 \pm 1)f_0$ at $\nu = 5/2$ and $(7 \pm 1.5)f_0$ at $\nu = 7/2$; see Sec. II and also Sec. S1 of the Supplemental Material [34]). While there is some indication of such a splitting in Fig. 7(e), it is far from conclusive. In general, such an indirect inference is complicated. In order to achieve the required resolution, it requires a sufficiently large magnetic field range that should be employed in the FFT, which at the same time makes the data more susceptible to low-frequency noise; see Fig. 7(d) versus 7(e).

Nevertheless, this limitation does not preclude us from studying the fermion parity stability in the temporal domain by repeated sweeps within a limited magnetic field interval, with the results shown in Fig. 8. Their reproducibility includes their phase which remains stable over several hours. What is even more remarkable is that when the phase of the oscillations fluctuates, it happens predominantly through phase jumping by π, as can be seen in Figs. 8 and 9(a). A π shift in the oscillations attributable to the $e/4$ particles can come from two distinct sources. The two scenarios correspond to the fluctuating parity of either neutral fermions or non-Abelian $e/4$ particles inside the interferometer. To better clarify the difference between these mechanisms, we remind the reader that we attribute the high-frequency oscillations not to the AB interference *per se* but rather to the switching of the interference signal on again, off again when the number of $e/4$ particles inside the interferometer loop changes from even to odd and back to even in response to the changing magnetic field. A stray

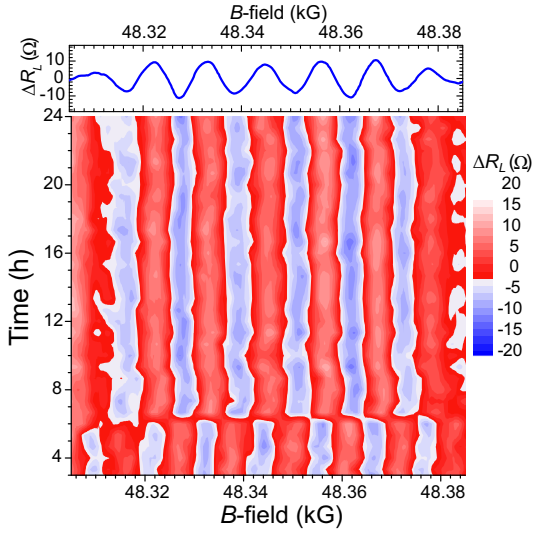

FIG. 8. Color plot of ΔR_L as a function of the magnetic field (x axis) and time in hours (y axis) for a representative interference measurement near $\nu = 7/2$. This plot represents the total of 76 up and down magnetic field sweeps similar to those of Fig. 3(b) (for a different sample preparation) but with the background subtracted, plotted as a function of the time to demonstrate the stability of the oscillations. A π phase jump occurs at about 6 hours, and for the following 18 hours the oscillation set is stable (sample 6, preparation 25, device type b, $T \sim 25$ mK).

$e/4$ quasiparticle tunneling into or out of the active area shifts this pattern by half a period due to the change in the parity of these quasiparticles. Meanwhile, the fermionic parity is the combined property of an even number of $e/4$ quasiparticles; it determines the sign of the interference contribution whenever it is present; its fluctuations would flip this sign. Hence, while both mechanisms would result in the oscillations shifted by π, there is, in principle, a difference in their signatures: Fluctuations in the number of $e/4$ particles would result in a purely "horizonatal" shift of the oscillations, whereas in the case of fluctuating fermionic parity one would expect a "vertical" reflection of these oscillations about either their peak or their minimum values. Such π jumps can be seen in Fig. 9, with the observed jumps shown in Figs. 9(a) and 9(b) seemingly resemble those resulting from the fluctuations in the number of $e/4$ particles. Figure 9(a) represents three different magnetic field sweeps taken over eight hours, each individual trace takes about 100 min. Two of them are perfectly in phase, while the third one displays a π phase jump whose location is indicated by an arrow. Two more sweeps performed in the same sample clearly show a similar π phase jump in Fig. 9(b). In the meantime, the π shift seen in Fig. 9(c) appears more consistent with the fluctuating fermionic parity. Definitive discrimination between these mechanisms, however, requires a more systematic study: The out-of-phase regions of oscillations seen in Fig. 9(c) also appear to be related to one another by a horizontal shift (rather than vertical reflection); such a

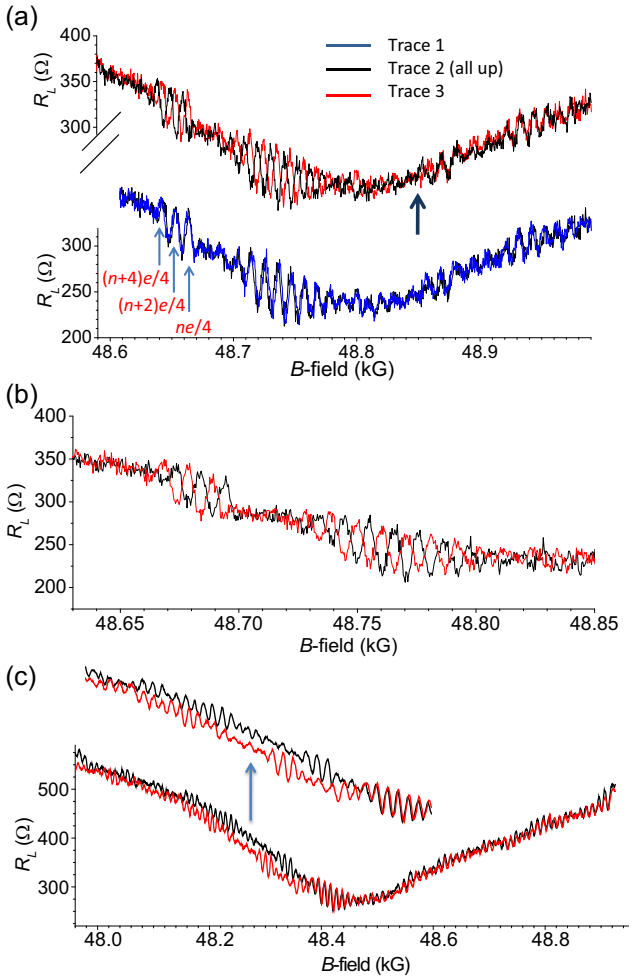

FIG. 9. π phase shifts in high-frequency oscillations at $\nu = 7/2$: (a) three consecutive magnetic field upsweeps taken near $\nu = 7/2$ as in Fig. 7 from the same sample but of a different preparation (sample 6, preparation 19, device type b, $T \sim 20$ mK). Traces 1 and 2 [bottom of panel (a)] overlap, whereas in trace 3 [top of panel (a) shown alongside trace 2 repeated for comparison] a π phase jump occurs in the time intervening trace 2 and 3 as this phase difference is apparent from the lowest shown B-field up to about 48.85 kG (marked by an arrow), at which point the phase reverts to that of trace 2. (See also Supplemental Material Sec. S5d [34].) (b) Two downsweeps [same sample and preparation, sweeps separated by days from (a)]. The two traces of R_L oscillations are out of phase by π. The π phase jump seemingly occurs away from the depicted oscillations showing the full extent of the sweep. (c) Consecutive downsweeps from the same sample and preparation [hours apart between the sweeps but days prior to the sweeps in panels (a) and (b)].

study is currently under way. Similar behavior is also observed at $\nu = 5/2$: Runs of reproducible oscillations are punctuated by occasional π shifts, the predominant instability; see Fig. 10 and Sec. S5d of the Supplemental Material Figs. S5-14 and S5-15 [34].

This direct observation of the oscillation stability gives us the means of establishing the temporal stability, the

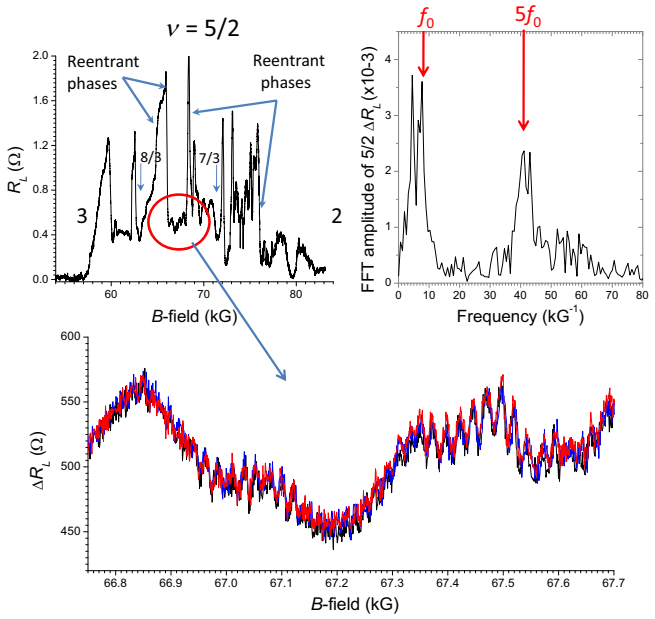

FIG. 10. Interference oscillations and their spectrum at $\nu = 5/2$. The top left panel shows the trace of R_L from filling factor $\nu = 3$ to 2; its enlargement in the vicinity of $\nu = 5/2$ (circled area) is shown in the bottom panel, with the corresponding FFT spectrum shown above in the right panel. f_0 is the frequency of oscillations observed at integer filling in the same sample. The lower panel shows three B-field sweeps in a single direction, demonstrating significant overlap of the resistance oscillations. The frequency of rapid oscillations is approximately $5f_0$ shown in the power spectrum. Each trace is 60 minutes, so the total data collection time is 6 hours (the opposite sweep direction is not shown). Sample 6, preparation 18, device type b, $T \sim 20$ mK.

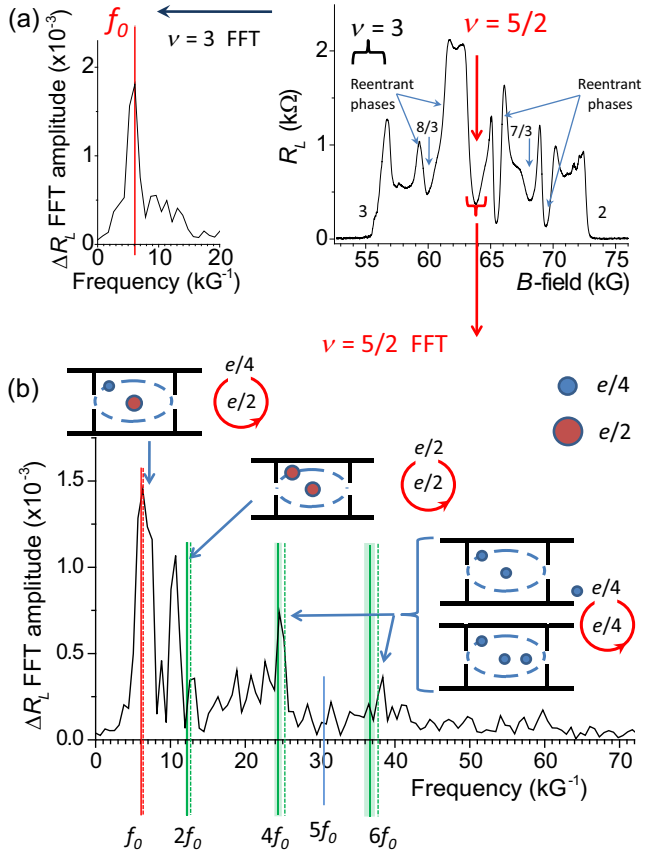

FIG. 11. Extracting power spectra in B-field sweeps and interference spectra at $\nu = 5/2$: (a) transport (R_L) through an interference device shown in Fig. 2, bottom micrograph (device type b), between filling factors $\nu = 2$ and 3 in a high-mobility heterostructure without additional Al purification. The power spectrum is extracted from a B-field sweep as follows: The background resistance near $\nu = 3$ is subtracted, after which a FFT is applied to the residual oscillations, producing the power spectrum that shows a principal peak at roughly 6 kG^{-1}, the frequency identified as f_0 whose value is closely matched at other integral filling factors. See also Fig. S5-1 in the Supplemental Material [34]. Temperature approximately 20 mK, sample 2, preparation 2, device type b. (b) Power spectrum of $R_L(B)$ near $\nu = 5/2$. The FFT window is bracketed in panel (a). After background subtraction and application of the FFT, four dominant peaks located near f_0, $2f_0$, $4f_0$, and $6f_0$ can be discerned. Here, f_0 is the frequency of the Aharonov-Bohm oscillations in the integer quantum Hall state [panel (a)], and marked in panels (a) and (b) by the solid red vertical line. Solid green lines in panel (b) indicate multiples of that frequency with the shaded area around them indicating the potential error margins stemming from the error of $\pm 1/8$ kG^{-1} in determining f_0. In the meantime, the dashed lines indicate multiples of the actual frequency of the first peak in panel (b).

magnetic field dependence of that stability by examining different magnetic field intervals, and influence of a host of other parameters, such as different gating configurations. The fact that we can actually see the rare phase jumps and assign their characteristic timescale is significant: This timescale provides the lower bound for the fermion parity stability which, in turn, not only further validates our theoretical model but may also have profound consequences for the future of such systems in quantum computation. After all, the fermion parity is supposed to encode the state of a topological qubit; its remarkable stability is a key to its potential utility.

Given the potential importance of the π phase jumps, it is essential to ask what experimental parameters can control their incidence and prevalence. One parameter conceivably influencing these π phase jumps—the density of encircled $e/4$ quasiparticles—can be estimated from the collected data. By simply counting of the $7f_0$ oscillation periods from the center of the 7/2 FQH plateau, and using f_0 to determine area A (see Fig. 11), we estimate their density to be approximately 170 μm^{-2} toward the edge of the plateau. This puts their separation at approximately 0.07 μm = 70 nm for the maximum density, which corresponds to about five magnetic lengths at these magnetic fields. (For more details on the calculations, see Supplemental Material Sec. S5d [34].) This suggests that the oscillations occur over a range of reasonable separations between $e/4$

quasiparticles. Yet, it does not provide any indication of a critical density that should trigger phase jumps.

We should comment in passing on the crucial difference between these π shifts and the phase jumps reported in Ref. [41]. The latter jumps are purportedly the consequence of charged Laughlin quasiparticles appearing within the active area of an interferometer as a consequence of changing magnetic field. In our case, due to the different energetics, the number of charge-$e/4$ quasiparticles is changing continuously with magnetic field and is causing the observed oscillations. Meanwhile, the π jumps occur either due to the fluctuating number of neutral fermions or stray charge-$e/4$ quasiparticles, which are expected in both $\nu = 5/2$ and $\nu = 7/2$ states. In the former scenario, the number of fermions cannot be systematically changed by varying the magnetic field due to their neutrality. In the latter scenario, this mechanism may be driven by $e/4$ particles trapped at some deep-lying impurity levels. In both scenarios, such fluctuations may occur even at a constant field, in which case they will manifest themselves as an extremely low-frequency telegraph noise revealed by a vertical cut through the color plot of Fig. 8.

C. Interference oscillations at $\nu = 5/2$

We now turn our attention to the interference oscillations observed at $\nu = 5/2$. The interference oscillations observed at this filling fraction in the devices with high Al purification strongly resemble those at $\nu = 7/2$. As shown in Fig. 10, these oscillations are remarkably stable and occur at 5 times the reference frequency f_0, which is once again indicative of the non-Abelian even-odd effect. Notice that another prominent spectral feature is located near f_0 itself.

Before we examine the spectra in more detail, it worth reiterating that the highest predicted oscillation frequency for Abelian AB interference at $\nu = 5/2$ is $2f_0$; any significant spectral weight at higher frequencies (specifically, within the range between $4f_0$ and $6f_0$ for $\nu = 5/2$) that is not a result of noise is an indicator of a non-Abelian nature of the state. Specifically, it should be interpreted as the evidence of the even-odd effect, which is a consequence of the quasiparticles' statistics and not charge; a naive application of Eq. (2) to the $e/4$ quasiparticles at $\nu = 5/2$ while neglecting their non-Abelian nature would instead result in the oscillations frequency of $2.25f_0$ in the Moore-Read state and $2.75f_0$ in the anti-Pfaffian state. For the genuinely Abelian candidate states, these frequencies would be f_0 in the $K = 8$ state and $3.5f_0$ in the (3,3,1) state [16]. [At $\nu = 7/2$, the respective frequencies would be $3.25f_0$ in the Moore-Read state, $3.75f_0$ in the anti-Pfaffian state, $1.5f_0$ in the $K = 8$ state, and $5f_0$ in the (3,3,1) state, all significantly below $7f_0$.] We can discard the possibility of multiple windings which would, in theory, result in higher frequency of interference oscillations. The amplitude of those contributions would be negligible as they require multiple tunneling across relatively wide constrictions.

While we empirically attribute the substantially more prominent high-frequency oscillations associated with the even-odd effect to the improved Al purity of the newer heterostructures, we emphasize that samples without this high Al purity can still demonstrate high-frequency oscillations at $\nu = 5/2$ as reported in the earlier work [22]. The focus of those studies was only on the oscillations associated with the even-odd effect; in the meantime, recent improvements in those materials and devices (without the Al-purity change) have provided higher-quality samples with better-defined FQH states of interest. This in turn allows for larger Fourier-transform windows, letting us focus on the finer details of the oscillation spectra, including their low-frequency features, than was possible in the previous studies. The results of such a study of the full spectral frequencies follow here.

A representative Fourier spectrum of the oscillations at $\nu = 5/2$ is shown in Fig. 11(b) along with the possible interpretation of its most prominent features. The oscillations in R_L around filling fraction $\nu = 3$ are used to determine the integer Aharonov-Bohm interference frequency f_0; details of the FFT analysis and magnetic field window size used for each FFT in results are described in

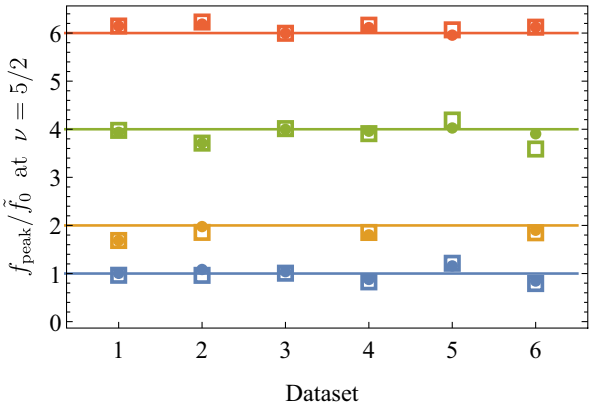

FIG. 12. Frequencies corresponding to the most prominent spectral peaks at $\nu = 5/2$ in six different datasets from different samples and preparations. Frequencies are normalized by $\tilde{f}_0$, which is the parameter obtained by applying linear fit to each observed set of peak frequencies (shown in circles) with the assumption that they correspond to integer multiples of this fundamental frequency. Open squares correspond to the frequencies obtained by taking the average value of the two frequencies that mark the width at half maximum for each peak, normalized by the same coefficients. The dataset identification is as follows: 1, sample 2, preparation 2; 2, same sample and preparation four days later; 3, sample 2, preparation 1; 4, sample 5, preparation 2; 5, sample 3, preparation 1; 6, sample 4, preparation 1. Note that two of the samples do not exhibit peaks at or near $2f_0$; cf. traces in Figs. 14(a) and 14(b) corresponding to datasets 3 and 2 shown here. $T \sim 20$ mK.

TABLE II. Comparison of frequencies $\tilde{f}_0$ obtained from linear fit of the $\nu = 5/2$ spectral data to f_0 observed at $\nu = 3$ for each sample and preparation.

$\tilde{f}_0$ (kG^{-1})	f_0 (kG^{-1})	Sample and preparation
6.2	6	Sample 2, prep 2
5.8	$6\frac{1}{2}$	Sample 2, prep 2, later
6.3	7	Sample 2, prep 1
10.0	$9\frac{1}{4}$	Sample 5, prep 2
4.5	$4\frac{3}{4}$	Sample 3, prep 1
4.7	$4\frac{1}{2}$	Sample 4, prep 1

Sec. S3 of the Supplemental Material [34]. The observed spectral peaks are located near f_0, $2f_0$, $4f_0$, and $6f_0$, with f_0 being the aforementioned reference frequency. (See Sec. S5f of the Supplemental Material [34] for more details on peak identification.) In order to verify this identification of the observed peaks, in Fig. 12 we plot their actual locations vs integer factor m that we assign to these peaks in five different samples, with two different preparations for one of the samples—six datasets altogether. Each set of observed peak frequencies at $\nu = 5/2$ is rescaled by the coefficient $\tilde{f}_0$ obtained from linear fit for each sample's frequency data. We can then compare $\tilde{f}_0$ obtained from linear fit to frequency f_0 corresponding to spectral peaks measured at $\nu = 3$ for each sample and preparation; the results of this comparison are shown in Table II.

The peak locations shown in Fig. 12 correspond to the highest measured values of spectral peaks. In Figs. S5-20 and S5-21 in the Supplemental Material [34], we present a comparison between two peak identification processes, one identifying peak locations by their highest value and the other using the average of the two points corresponding to their half values. The observed features are consistent with the expectations for both Abelian and non-Abelian interference processes due to charge-$e/4$ and charge-$e/2$ quasiparticles. (We remark that the peak identification procedure used here is the same as was illustrated earlier in Fig. 4 showing the comparison of actual traces and their Fourier transforms for $\nu = 4$ and $\nu = 16/5$, further strengthening our confidence in identification of observed spectral features.)

In the power spectrum presented in Fig. 11(b), the amplitudes of these four peaks drop progressively with the frequency, a common property of these spectra in our study, but with exceptions (see Supplemental Material Fig. S5-16 [34]). The base frequency f_0 depends on the size of the interferometer, as seen by comparing the power spectra from different devices, but the ratios of the power spectrum positions remain close to 1:2:4:6. (Note that the base frequency f_0 can be measured at the different integer filling factors, a property of AB oscillations, and this is demonstrated in the Supplemental Material Figs. S4-1 and S4-2 [34].) The spectral features shown in Fig. 11(b) are sharp, in part due to the low temperature of 20 mK, but also due to the details of construction of this particular interferometer. Larger devices have larger separation in the spectral features (since $f_0 \propto A$) and, consequently, better resolution, but the amplitudes of the higher-frequency features at $4f_0$ and $6f_0$ are reduced in the largest devices tested. A repetition of this measurement on the same device but days later is shown in Fig. 14(b) (presented there as a part of another study to be discussed later), with the dominant peaks persisting at the same frequencies. Further $5/2$ power spectra are displayed in the Supplemental Material Figs. S5-16 and S5-17 [34].

Before attempting a similar analysis of the finer spectral features of interference oscillations at $\nu = 7/2$ accessible through a wider Fourier-transform window, let us reiterate that the common observed feature in multiple sample preparations, interference measurements, and their respective spectra such as those shown in Figs. 3(c) and 7 [with another example shown in Fig. 13(b) and more spectra presented in Sec. S5c of the Supplemental Material [34]] is the large spectral weight concentrated around $7f_0$, the frequency of the predicted even-odd effect. Yet upon closer inspection of the spectrum in Fig. 7(e), another common feature appears to be a sharp minimum right at that frequency $7f_0$. (A similar feature is also observed in samples at $\nu = 5/2$; see, e.g., Fig. S6-2 in the Supplemental Material [34].) The most likely origin for this dip is some low-frequency modulation of the even-odd oscillations. Irrespective of its origin, such a modulation would split the high-frequency Fourier peak into two resulting in a spectral minimum at the location of the original peak. The visibility of this minimum then becomes a function of the frequency window used in the Fourier transform; this effect can be clearly seen in Fig. 7 where a prominent spectral peak at $7f_0$ seen in Fig. 7(d) evolves into a pronounced minimum seen in Fig. 7(e) as the size of the FFT window is increased in an attempt to tease out finer spectral features from the dominant peak. As we mention in the Introduction, the $e/4$-$e/2$ interference with fixed fermion parity would result in a split peak $(7 \pm 1.5)f_0$. However, there are also other potential, if less systematic, sources of low-frequency modulation of the dominant $7f_0$ frequency such as potential dependence of the oscillation amplitude on the distance from the overall resistance minimum marking the QH state. Such a modulation is discussed in Sec. S5g of the Supplemental Material [34]; the corresponding spectral feature at about $0.4f_0$ is encircled in Fig. 7(e). The modulation by $0.4f_0$, is then combined with the modulation by $1.5f_0$ due to $e/4$-$e/2$ interference oscillations. The comparison between the actual observed spectrum and the spectrum modeled by including both of these modulations is shown in Figs. 13(b) and 13(d). Note that the model uses a finite Fourier-transform window similar to that used in processing the experimental data. For comparison, Figs. 13(a) and 13(c)

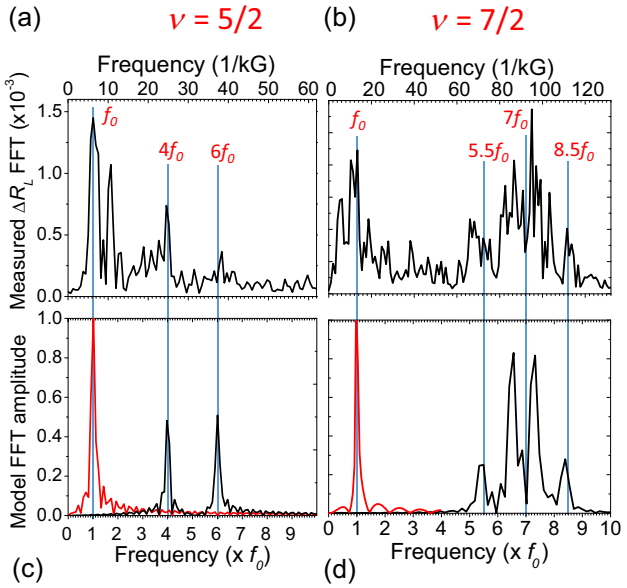

FIG. 13. Modeling FFT spectra at $\nu = 5/2$ and $7/2$. In a magnetic field sweep at $\nu = 5/2$ and $\nu = 7/2$, rapid oscillations due to the even-odd effect will be modulated by slower oscillations due to $e/4$-$e/2$ interference. At $\nu = 5/2$ this implies modulating oscillations at $5f_0$ by oscillations at f_0, resulting in peaks at $4f_0$ and $6f_0$. At $\nu = 7/2$, $1.5f_0$ modulation of $7f_0$ even-odd oscillations should produce peaks at $5.5f_0$ and $8.5f_0$. Panels (a) and (b) show measured power spectra at these filling fractions: (a) $\nu = 5/2$, sample 2, preparation 2 [same as in Fig. 11(b)]; (b) $\nu = 7/2$, sample 6, preparation 15, device type b; $T \sim 20$ mK in both cases. The measured power spectra are compared with simple models. The black trace in panel (c) is the FFT of the expression $\Delta R_L = \cos(2\pi B f_0) \times \cos[2\pi B(5f_0)]$ taken using the magnetic field window similar to the one used to obtain power spectra in the experiment. The red trace is the FFT of $\Delta R_L = \cos(2\pi B f_0)$ demonstrating the f_0 oscillation peak. The spectra are scaled to match the locations and amplitudes of their peaks at frequency f_0. Panel (d) shows a similar modulation of the $7f_0$ even-odd oscillations by $1.5f_0$ oscillations expected for the $e/4$-$e/2$ interference at $\nu = 7/2$. In addition, the minima of R_L are reproducibly formed away from the reentrant quantum Hall phases in the high-quality material used in this study, resulting in an additional low-frequency modulation at about $0.4f_0$. To capture these effects, we model the resistance as $\Delta R_L = \{0.25\cos[2\pi B(0.4f_0)] + 0.75\cos[2\pi B(1.5f_0)]\} \times \cos[2\pi B(7f_0)]$. The FFT of this expression results in the spectrum shown in panel (d), compared directly to measured data at $\nu = 7/2$ in panel (b). Again, a FFT of $\Delta R_L = \cos(2\pi B f_0)$ is the red trace panel (d). (See also Supplemental Material Sec. S5g and Fig. S5-23 [34].).

show the observed and modeled spectra at $\nu = 5/2$ where only the modulation due to $e/4$-$e/2$ interference is taken into account.

D. Abelian interference oscillations at $\nu = 5/2$ and $7/2$

While the high-frequency oscillations are of foremost importance for demonstrating the non-Abelian nature of the $\nu = 5/2$ and $7/2$ states, the low-frequency features that we investigate in this study also reveal some important information. We should mention that the ability to discern lower-frequency spectral features is another key new element of the present study; in the past, they were hard to extract due to the narrow magnetic field range where these oscillations had been seen. Utilizing higher-purity heterostructures and somewhat different interferometer design, we are able to better isolate the quantum Hall state at $\nu = 5/2$ from the surrounding compressible states, which results in more pronounced, broader minima in R_L supporting longer runs of higher-amplitude interference oscillations than before. This allows us to observe and analyze those lower-frequency spectral features, thus addressing one of the shortcomings of our earlier study [22].

It is instructive to compare the low-frequency features between the $\nu = 5/2$ and $7/2$ states. The two states are theoretically expected to correspond to the same topological order, with the same charge and statistics of its excitations. However, due to its different filling factor, the periodicity of AB interference at $\nu = 7/2$ is expected to be different from $5/2$, as can be seen from Eqs. (2) and (3). Specifically, the interference of $e/4$ edge excitations around $e/2$ bulk quasiparticles should now occur with the periodicity of $2\Phi_0/3$ (instead of Φ_0), and thus the expected spectral peak at $1.5f_0$, nicely distinguishing it from potential electron contribution still occurring at f_0. Lastly, $e/2$-$e/2$ interference should manifest itself through a peak at $3f_0$. The oscillation spectrum shown in Fig. 7(e) is consistent with these expectations. See also Sec. S5c of the Supplemental Material [34].

The f_0 spectral peak at $\nu = 5/2$ decays rapidly with increasing temperature up to $T \approx 80$ mK, which is roughly the onset temperature of the deep minimum in R_L. (See Supplemental Material Sec. S5i, Figs. S5-26 and S5-27 [34] for more details.) This strongly implies that oscillations at this frequency are, indeed, due to the physics of this fractional quantum Hall state. In particular, this hints at the $e/4$-$e/2$ interference contribution to these oscillations, in addition to the omnipresent electron contribution.

The last process whereby $e/2$ quasiparticles braid around bulk $e/2$ quasiparticles should result in spectral features at $2f_0$ for $\nu = 5/2$ and at $3f_0$ for $7/2$. While the observed oscillation spectra at $\nu = 7/2$ contain hints of the $3f_0$ feature (see, e.g., Fig. S5-10 of the Supplemental Material [34] for the best example), Fig. 7 illustrates the problematic nature of reliably discerning this feature from the noisy background. In the meantime, its $2f_0$ counterpart in the $\nu = 5/2$ spectra obtained in the samples without additional Al purification appears far more prominent, as can been seen in Fig. 11. We should note that this feature is systematically seen at frequencies somewhat below $2f_0$; see, e.g., Fig. 12 showing its observed position for four different samples and preparations. While we are not certain about the reasons for this discrepancy (it is a

subject of an ongoing study), the prominence of this spectral feature enables us to implement additional tests. An important property of the observed $\nu = 5/2$ oscillation spectra presented here is changing of the magnitude of the $2f_0$ peak as a function of the separation between the inner edge currents in the backscattering constrictions (distance d in schematic of Fig. 2). Figures 14(a) and 14(b) show two complete power spectra in the same interferometer at $\nu = 5/2$ but with different applied voltages V_b and V_s: The more negative the V_b value is, the narrower the constrictions acting as "beam splitters" are, which should change the backscattering (tunneling) amplitudes. V_s can be adjusted so that for two different V_b values, the interferometer areas A are kept essentially the same. Standard longitudinal resistance (R_L) measurements (see Supplemental Material Sec. S5h, Fig. S5-25 [34]) show little difference for the two different gate configurations. Note that in the device with voltage $V_b = -3.5$ V, the $2f_0$ peak is essentially absent, whereas in the device with $V_b = -9.0$ V a large $2f_0$ peak is present. We therefore conclude that the width d of the constriction (the separation between the QH edges; see Fig. 2) is an important factor controlling the presence of the peak at $2f_0$. The V_b voltages are adjusted to a range of values between the two shown in the full spectra of Figs. 14(a) and 14(b); the resulting plot of the measured ratio between the peak amplitudes at $2f_0$ and f_0 as a function of V_b is shown in Fig. 14(c). According to our findings, as V_b becomes more negative (the backscattering distance d becomes smaller), the amplitude ratio increases. This finding is consistently observed in multiple different heterostructure wafers and multiple different devices. (We expect a similar behavior of the $3f_0$ peak at $\nu = 7/2$ but have not performed this study; it is a subject of ongoing research.)

This result can be understood as a consequence of the difference in tunneling probability of $e/4$ and $e/2$ edge excitations as a function of the tunneling distance d between the edges in the constrictions that form the interferometer. Theoretical analysis of the tunneling process of the excitations at $5/2$ predicts that the amplitude of the $e/2$ tunneling process is suppressed by comparison to the $e/4$ tunneling due to the larger momentum transfer required for backscattering at a gated narrowing, with the effect becoming more pronounced as the tunneling distance increases [16]. This effect is illustrated in Ref. [46] where the dependence of the ratio between the $e/4$ and $e/2$ tunneling amplitudes as a function of the tunneling distance has been investigated numerically for the Moore-Read state. Our experimental findings are consistent with this picture, showing the amplitude of the $2f_0$ peak attributed to the $e/2$ interference decreasing much faster with the distance than that of the peak at f_0. Note that the physics behind this effect should be insensitive to the precise nature of the $\nu = 5/2$ state; it is a consequence of the difference between different quasiparticles' charges. This should be contrasted with the temperature and bias voltage dependence

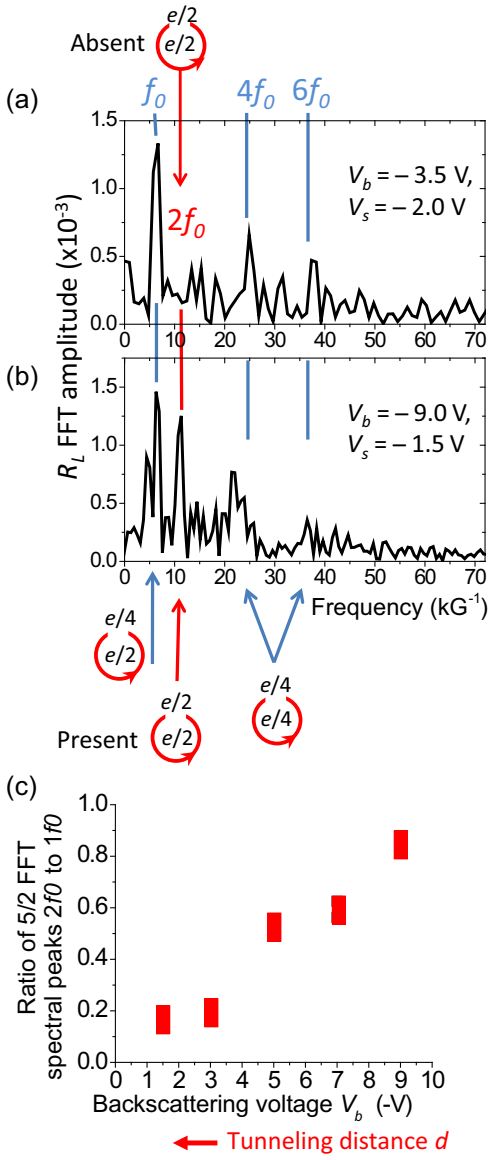

FIG. 14. (a),(b) $\nu = 5/2$ oscillation spectra at two different gate-voltage settings (sample 2, preparations 1 and 2, device type b, $T \sim 20$ mK). The spectrum in panel (b) shows four peaks at f_0, $2f_0$, $4f_0$, and $6f_0$, consistent with $e/4$ and $e/2$ interference. The $2f_0$ peak is absent when the backscattering gate voltage V_b is changed from -9 to -3.5 V, increasing the tunneling distance d for interfering quasiparticles. The side-gate voltage V_s is adjusted to preserve the area A. (Supplemental Material Sec. S5h, Fig. S5-25 [34] demonstrate the overall similar transport between $\nu = 2$ and 3 for these gate settings.) (c) Ratio of the peak value at $2f_0$ to that at f_0 for a series of backscattering gate voltages V_b in the same device (sample 2, preparations 1 to 5, $T \sim 20$ mK). The increase of the peak amplitude ratio in response to the constriction narrowing (more negative V_b) may be reflecting relative tunneling amplitudes for $e/2$ and $e/4$ quasiparticles.

of these tunneling processes, which is expected to be governed by the quasiparticles' scaling exponents. Those considerations would lead to different predictions for the anti-Pfaffian vs both the Moore-Read and the PH-Pfaffian

states, potentially allowing for discriminating between these states [16]. Our study is not sensitive to this distinction.

We should also comment here that contrary to the analysis of Ref. [39], we do not expect to be able to distinguish between the Moore-Read, anti-Pfaffian, and PH-Pfaffian states based on the location of the high-frequency spectral peaks. For the reasons mentioned earlier (and further elaborated in the Supplemental Material [34]), the Abelian phase associated with the $e/4$-$e/4$ braiding (which is different in these states) does not directly contribute to the AB phase observed in the experiment; the interference itself is destroyed if an $e/4$ quasiparticle braids another unpaired one, whereas only the overall fusion channel matters for paired ones. Therefore, the observed high-frequency peaks are merely indicative of the non-Abelian nature of the state, but their positions cannot be used to discriminate between the candidate states. That said, they contain the information about temporal stability of the non-Abelian fusion channels. For the case of stable overall fermion parity at $\nu = 5/2$, we expect to see peaks at $4f_0$ and $6f_0$. This scenario appears to be in agreement with the observed enhanced spectral features at these frequencies reported here. However, in both past [22] and present studies (see Sec. S6 of the Supplemental Material [34]), some sweeps result in only a $5f_0$ peak, consistent with random (but not rapidly fluctuating) fusion channel of additional pairs of $e/4$ quasiparticles introduced into the interferometer. The conditions that affect the temporal stability of the fermion parity are the subject of future investigation.

V. SUMMARY AND CONCLUSIONS

Using magnetic field sweeps in quantum Hall Fabry-Pérot interferometers at $\nu = 5/2$ and $7/2$ filling, we observe large amplitude, reproducible interference oscillations at frequencies inconsistent with Abelian Aharonov-Bohm interference but specific for the non-Abelian even-odd effect for the respective quantum Hall states. With new ultrahigh-purity heterostructures, we observe such oscillations for the first time in the $\nu = 7/2$ QH state, providing the first evidence for the non-Abelian statistics of its charge-$e/4$ excitations. Furthermore, the oscillations attributed to the non-Abelian $e/4$ quasiparticles are shown to be remarkably stable, indicating stability of their fusion channel—the fermion parity—which in turn may have profound consequences for their applications for topological quantum computation. This interpretation is further strengthened by the observation of occasional π phase jumps, the predominant type of instability observed in our traces. These are consistent with the change of either the fermion parity or the parity of non-Abelian charge-$e/4$ quasiparticles inside the interferometer, both of which should manifest themselves in a π phase shift of the oscillations. Moreover, the fact that we observe them infrequently and can actually associate a timescale (hours) to the parity flips is perhaps the most promising outcome of our study, demonstrating the potential of such quantum Hall systems for quantum computing.

The Fourier transforms of the magnetic field dependence of the resistance around those filling factors show not only peaks corresponding to the non-Abelian even-odd effect associated with $e/4$ quasiparticles but also a set of spectral peaks consistent with those anticipated for all possible combinations of interfering quasiparticle types expected to be present in these systems, thus also accounting for the Abelian interference effects.

In our study, we also demonstrate means of controlling the interference processes. The Abelian $e/2$-$e/2$ interference is shown to be suppressed by reducing the edge quasiparticle backscattering, thus allowing us to distill different contributions to the interference oscillations. This gate control is presently the subject of intense investigation, and these are essential steps in an effort to develop devices for topological quantum computation.

ACKNOWLEDGMENTS

We are grateful for some illuminating discussions with D. E. Feldman and B. I. Halperin as well as with Parsa Bonderson, who has also been our coauthor on related earlier projects. We acknowledge the hospitality of KITP supported in part by the NSF under Grant No. NSF PHY-1748958. We also acknowledge the Aspen Center for Physics, which is supported by the NSF under Grant No. NSF PHY-1607611. The work at Princeton University (L. N. P., K. W. W., K. W. B.) was funded by the Gordon and Betty Moore Foundation through the EPiQS initiative Grants No. GBMF4420 and GBMF9615 (L. N. P.), and by the National Science Foundation MRSEC Grant No. DMR 1420541 (Y. J. C.).

[1] C. Nayak, S. H. Simon, A. Stern, M. Freedman, and S. Das Sarma, *Non-Abelian Anyons and Topological Quantum Computation*, Rev. Mod. Phys. **80**, 1083 (2008).

[2] G. Moore and N. Read, *Nonabelions in the Fractional Quantum Hall Effect*, Nucl. Phys. **B360**, 362 (1991).

[3] S.-S. Lee, S. Ryu, C. Nayak, and M. P. A. Fisher, *Particle-Hole Symmetry and the $\nu = 5/2$ Quantum Hall State*, Phys. Rev. Lett. **99**, 236807 (2007).

[4] M. Levin, B. I. Halperin, and B. Rosenow, *Particle-Hole Symmetry and the Pfaffian State*, Phys. Rev. Lett. **99**, 236806 (2007).

[5] P. Bonderson, C. Nayak, and X.-L. Qi, *A Time-Reversal Invariant Topological Phase at the Surface of a 3D Topological Insulator*, J. Stat. Mech. 2013, P09016 (2013).

[6] X. Chen, L. Fidkowski, and A. Vishwanath, *Symmetry Enforced Non-Abelian Topological Order at the Surface of a Topological Insulator*, Phys. Rev. B **89**, 165132 (2014).

[7] D. T. Son, *Is the Composite Fermion a Dirac Particle?*, Phys. Rev. X **5**, 031027 (2015).

[8] P. T. Zucker and D. E. Feldman, *Stabilization of the Particle-Hole Pfaffian Order by Landau-Level Mixing*

and Impurities That Break Particle-Hole Symmetry, Phys. Rev. Lett. **117**, 096802 (2016).

[9] C. Nayak and F. Wilczek, *2n-Quasihole States Realize 2^{n-1}-Dimensional Spinor Braiding Statistics in Paired Quantum Hall States*, Nucl. Phys. **B479**, 529 (1996).

[10] N. Read and D. Green, *Paired States of Fermions in Two Dimensions with Breaking of Parity and Time-Reversal Symmetries and the Fractional Quantum Hall Effect*, Phys. Rev. B **61**, 10267 (2000).

[11] M. Milovanovic and N. Read, *Edge Excitations of Paired Fractional Quantum Hall States*, Phys. Rev. B **53**, 13559 (1996).

[12] E. Fradkin, C. Nayak, A. Tsvelik, and F. Wilczek, *A Chern-Simons Effective Field Theory for the Pfaffian Quantum Hall State*, Nucl. Phys. **B516**, 704 (1998).

[13] A. Stern and B. I. Halperin, *Proposed Experiments to Probe the Non-Abelian $\nu = 5/2$ Quantum Hall State*, Phys. Rev. Lett. **96**, 016802 (2006).

[14] P. Bonderson, A. Kitaev, and K. Shtengel, *Detecting Non-Abelian Statistics in the $\nu = 5/2$ Fractional Quantum Hall State*, Phys. Rev. Lett. **96**, 016803 (2006).

[15] P. Bonderson, K. Shtengel, and J. K. Slingerland, *Interferometry of Non-Abelian Anyons*, Ann. Phys. (Amsterdam) **323**, 2709 (2008).

[16] W. Bishara, P. Bonderson, C. Nayak, K. Shtengel, and J. K. Slingerland, *Interferometric Signature of Non-Abelian Anyons*, Phys. Rev. B **80**, 155303 (2009).

[17] B. I. Halperin, A. Stern, I. Neder, and B. Rosenow, *Theory of the Fabry-Pérot Quantum Hall Interferometer*, Phys. Rev. B **83**, 155440 (2011).

[18] R. L. Willett, M. J. Manfra, L. N. Pfeiffer, and K. W. West, *Confinement of Fractional Quantum Hall States in Narrow Conducting Channels*, Appl. Phys. Lett. **91**, 052105 (2007).

[19] R. L. Willett, L. N. Pfeiffer, and K. W. West, *Measurement of Filling Factor 5/2 Quasiparticle Interference with Observation of Charge $e/4$ and $e/2$ Period Oscillations*, Proc. Natl. Acad. Sci. U.S.A. **106**, 8853 (2009).

[20] R. L. Willett, L. N. Pfeiffer, and K. W. West, *Alternation and Interchange of $e/4$ and $e/2$ Period Interference Oscillations Consistent with Filling Factor 5/2 Non-Abelian Quasiparticles*, Phys. Rev. B **82**, 205301 (2010).

[21] R. L. Willett, L. N. Pfeiffer, K. W. West, and M. J. Manfra, *Aharonov-Bohm Effect and Coherence Length of Charge $e/4$ Quasiparticles at 5/2 Filling Factor Measured in Multiple Small Fabry-Pérot Interferometers*, arXiv:1301.2594.

[22] R. L. Willett, C. Nayak, K. Shtengel, L. N. Pfeiffer, and K. W. West, *Magnetic-Field-Tuned Aharonov-Bohm Oscillations and Evidence for Non-Abelian Anyons at $\nu = 5/2$*, Phys. Rev. Lett. **111**, 186401 (2013).

[23] I. P. Radu, J. B. Miller, C. M. Marcus, M. A. Kastner, L. N. Pfeiffer, and K. W. West, *Quasi-Particle Properties from Tunneling in the $\nu = 5/2$ Fractional Quantum Hall State*, Science **320**, 899 (2008).

[24] V. Venkatachalam, A. Yacoby, L. Pfeiffer, and K. West, *Local Charge of the $\nu = 5/2$ Fractional Quantum Hall State*, Nature (London) **469**, 185 (2011).

[25] M. Dolev, M. Heiblum, V. Umansky, A. Stern, and D. Mahalu, *Observation of a Quarter of an Electron Charge at the $\nu = 5/2$ Quantum Hall State*, Nature (London) **452**, 829 (2008).

[26] M. Dolev, Y. Gross, Y. C. Chung, M. Heiblum, V. Umansky, and D. Mahalu, *Dependence of the Tunneling Quasiparticle Charge Determined via Shot Noise Measurements on the Tunneling Barrier and Energetics*, Phys. Rev. B **81**, 161303 (R) (2010).

[27] M. Carrega, D. Ferraro, A. Braggio, N. Magnoli, and M. Sassetti, *Anomalous Charge Tunneling in Fractional Quantum Hall Edge States at a Filling Factor $\nu = 5/2$*, Phys. Rev. Lett. **107**, 146404 (2011).

[28] D. E. Feldman and M. Heiblum, *Why a Noninteracting Model Works for Shot Noise in Fractional Charge Experiments*, Phys. Rev. B **95**, 115308 (2017).

[29] M. Banerjee, M. Heiblum, V. Umansky, D. E. Feldman, Y. Oreg, and A. Stern, *Observation of Half-Integer Thermal Hall Conductance*, Nature (London) **559**, 205 (2018).

[30] R. Bhattacharyya, M. Banerjee, M. Heiblum, D. Mahalu, and V. Umansky, *Melting of Interference in the Fractional Quantum Hall Effect: Appearance of Neutral Modes*, Phys. Rev. Lett. **122**, 246801 (2019).

[31] D. T. McClure, W. Chang, C. M. Marcus, L. N. Pfeiffer, and K. W. West, *Fabry-Pérot Interferometry with Fractional Charges*, Phys. Rev. Lett. **108**, 256804 (2012).

[32] F. E. Camino, W. Zhou, and V. J. Goldman, *Aharonov-Bohm Superperiod in a Laughlin Quasiparticle Interferometer*, Phys. Rev. Lett. **95**, 246802 (2005).

[33] F. E. Camino, W. Zhou, and V. J. Goldman, *$e/3$ Laughlin Quasiparticle Primary-Filling $\nu = 1/3$ Interferometer*, Phys. Rev. Lett. **98**, 076805 (2007).

[34] See Supplemental Material at http://link.aps.org/supplemental/10.1103/PhysRevX.13.011028 for supplemental data and commentary pertaining to each section of the paper.

[35] Y. Zhang, D. T. McClure, E. M. Levenson-Falk, C. M. Marcus, L. N. Pfeiffer, and K. W. West, *Distinct Signatures for Coulomb Blockade and Aharonov-Bohm Interference in Electronic Fabry-Pérot Interferometers*, Phys. Rev. B **79**, 241304(R) (2009).

[36] N. Ofek, A. Bid, M. Heiblum, A. Stern, V. Umansky, and D. Mahalu, *Role of Interactions in an Electronic Fabry-Pérot Interferometer Operating in the Quantum Hall Effect Regime*, Proc. Natl. Acad. Sci. U.S.A. **107**, 5276 (2010).

[37] J. Nakamura, S. Fallahi, H. Sahasrabudhe, R. Rahman, S. Liang, G. C. Gardner, and M. J. Manfra, *Aharonov-Bohm Interference of Fractional Quantum Hall Edge Modes*, Nat. Phys. **15**, 563 (2019).

[38] P. Bonderson, K. Shtengel, and J. K. Slingerland, *Probing Non-Abelian Statistics with Quasiparticle Interferometry*, Phys. Rev. Lett. **97**, 016401 (2006).

[39] C. W. von Keyserlingk, S. H. Simon, and B. Rosenow, *Enhanced Bulk-Edge Coulomb Coupling in Fractional Fabry-Pérot Interferometers*, Phys. Rev. Lett. **115**, 126807 (2015).

[40] B. Rosenow, B. I. Halperin, S. H. Simon, and A. Stern, *Bulk-Edge Coupling in the Non-Abelian $\nu = 5/2$ Quantum Hall Interferometer*, Phys. Rev. Lett. **100**, 226803 (2008).

[41] J. Nakamura, S. Liang, G. C. Gardner, and M. J. Manfra, *Direct Observation of Anyonic Braiding Statistics*, Nat. Phys. **16**, 931 (2020).

[42] I. Sivan, R. Bhattacharyya, H. K. Choi, M. Heiblum, D. E. Feldman, D. Mahalu, and V. Umansky, *Interaction-Induced Interference in the Integer Quantum Hall Effect*, Phys. Rev. B **97**, 125405 (2018).

[43] Y. J. Chung, K. W. Baldwin, K. W. West, M. Shayegan, and L. N. Pfeiffer, *Surface Segregation and the Al Problem in GaAs Quantum Wells*, Phys. Rev. Mater. **2**, 034006 (2018).

[44] Y. J. Chung, K. A. Villegas Rosales, H. Deng, K. W. Baldwin, K. W. West, M. Shayegan, and L. N. Pfeiffer, *Multivalley Two-Dimensional Electron System in an AlAs Quantum Well with Mobility Exceeding* 2×10^6 $\mathrm{cm^2\,v^{-1}\,s^{-1}}$, Phys. Rev. Mater. **2**, 071001(R) (2018).

[45] In magnetic field sweeps, R_L measurements at integer filling factors show AB interference oscillations that correspond to the addition of one flux quantum, and the period of these oscillations is Φ_0 with the fundamental frequency $f_0 = 1/\Phi_0$. For each preparation, such a measurement at integer filling factor is performed to establish this fundamental value for comparison. The fundamental frequency f_0 is independent of the integer filling factor (see Fig. S4-2 of Supplemental Material [34]). It is important to note that if a density shift occurs in the 2D electron system, this would affect the measured f_0 making comparison between interference features at different densities untenable.

[46] H. Chen, Z.-X. Hu, K. Yang, E. H. Rezayi, and X. Wan, *Quasiparticle Tunneling in the Moore-Read Fractional Quantum Hall State*, Phys. Rev. B **80**, 235305 (2009).